1967

Fatigue of 2024-T3 aluminum alloy due to broad-band and narrow-band random loading

Benny Max Hillberry
Iowa State University

67-8913

HILLBERRY, Benny Max, 1937-

FATIGUE OF 2024-T3 ALUMINUM ALLOY DUE TO BROAD-BAND AND NARROW-BAND RANDOM LOADING.

Iowa State University of Science and Technology, Ph.D., 1967
Engineering, metallurgy

University Microfilms, Inc., Ann Arbor, Michigan

FATIGUE OF 2024-T3 ALUMINUM ALLOY DUE TO BROAD-BAND AND NARROW-BAND RANDOM LOADING

by

Benny Max Hillberry

A Dissertation Submitted to the
Graduate Faculty in Partial Fulfillment of
The Requirements for the Degree of
DOCTOR OF PHILOSOPHY

Major Subjects: Mechanical Engineering
Electrical Engineering

Approved:

Signature was redacted for privacy.

In Charge of Major Work

Signature was redacted for privacy.

Heads of Major Departments

Signature was redacted for privacy.

Dean of Graduate College

Iowa State University
Of Science and Technology
Ames, Iowa

1967

TABLE OF CONTENTS

	Page
LIST OF SYMBOLS	iv
INTRODUCTION	1
REVIEW OF RELATED WORK	3
Cumulative Damage	3
Random Fatigue Tests	4
DESCRIPTION OF TEST FACILITY	7
Complete System	7
Specimen	12
Electrodynamic Shaker	16
Force Transducer	16
Filters	20
Broad-band filter	20
Narrow-band filter	21
DESCRIPTION OF RANDOM FATIGUE TESTS	24
Gaussian Noise	24
Power Spectral Density	24
Ratio of Zero Crossings with Positive Slope Per Second to Positive Peaks Per Second	26
Peak Probability Density Function	30
TEST RESULTS	35
Constant-Amplitude, Sine-Wave Fatigue Tests	35
Corten-Dolan Constant	35
Random Fatigue Tests	37

Page

PREDICTED FATIGUE LIFE 41

Palmgren-Miner Theory 41

Corten-Dolan Theory 47

Equivalent-Crack-Length Theory 55

Relation Between Broad-Band and Narrow-Band Loading 62

Comparison with Fuller's test results 65

CONCLUSIONS 67

RECOMMENDATIONS FOR FURTHER STUDY 69

LITERATURE CITED 71

ACKNOWLEDGMENTS 75

APPENDIX 76

Evaluation of $\int_0^\infty z^b W(z)\,dz$ 76

Narrow-band loading 76
Broad-band random loading 76

LIST OF SYMBOLS

A	material dependent constant for describing modified fatigue curve
B	material dependent constant for describing constant-amplitude, sine-wave fatigue curve
b	reciprocal of negative slope for constant-amplitude, sine-wave fatigue curve
d	Corten-Dolan constant which is reciprocal of negative slope for modified fatigue curve
D	fatigue damage
E( )	expected value of variable
F	material constant
f	frequency, cycles/sec.
G( )	power spectral density function
j	$\sqrt{-1}$
K	constant
K_1	$\sqrt{1 - \left(\frac{N_0}{M}\right)^2}$
K_2	$\frac{K_1}{\left(\frac{N_0}{M}\right)}$
ℓ	fatigue crack length
M	number of positive peaks per second
N	number of cycles to failure under constant-amplitude, sine-wave loading
n	number of cycles at given stress
N_g	total number of cycles to failure in Corten-Dolan theory

N_0	number of zero-crossings with positive slope per second
N_p	total number of positive peaks to failure
$N_{p>0}$	number of positive peaks greater than zero to failure
N'	number of cycles to failure defined by the Corten-Dolan fatigue curve
$P(\ )$	probability that variable will be exceeded
$S_{y.s.}$	yield strength of the material, ksi
$W(\ )$	peak probability density function
$Y(\ )$	transfer function of the system
z	standardized peak variable
σ_i	percentage of cycles at σ_i in Corten-Dolan theory
$\Gamma(\ )$	gamma function
θ	material constant
σ	stress amplitude for sine-wave loading, ksi
σ_p	stress peak in random loading, ksi
σ_{rms}	root mean square value of instantaneous stress, ksi
ω	angular frequency, rad/sec.

INTRODUCTION

A fatigue failure can result when a material is stressed repeatedly to a stress level much less than the ultimate strength. Wöhler (1, p. 12), prompted by railway axle failures, began his work in 1852. He was the first to establish the now familiar S-N curve. His method of testing, using the rotating beam machine, is still being used today. Since that time a great deal of research has been done on the fatigue behavior of metals. This research has been led by the ever increasing demands being placed on materials through higher design stresses and reduced factors of safety. With the developments of today becoming more complex, failures are more costly in time, money, and in some cases, loss of life. Fatigue failures are of primary concern to designers today.

Research on the basic mechanism of fatigue failure has not yielded a thorough understanding of fatigue and may not for years to come.

The many factors which influence the fatigue behavior, such as size, surface finish, stress concentration, etc., have been investigated, and the designer can make the necessary allowances. However, the stress-time histories encountered in service are much different than the constant-amplitude, sine-wave loading used in the laboratory to determine the fatigue properties. In many instances, particularily in aircraft structures, the stress varies randomly.

In this investigation, laboratory specimens of 2024-T3 aluminum alloy were subjected to broad- and narrow-band types of random loading in order to determine the effects of the broad-band random loading on the fatigue behavior. In addition, an attempt was made to determine which statistical quantities of the stress-history should be used in comparing different types of random loading.

The results are compared with the predicted fatigue life given by the Palmgren-Miner and the Corten-Dolan theories and also that given by a proposed equivalent-crack-length theory.

REVIEW OF RELATED WORK

Cumulative Damage

The cumulative damage concept of fatigue deals with predicting the number of cycles to failure when more than one stress amplitude is applied during the lifetime of the part. Palmgren (2) in 1924 and Miner (3) in 1945 independently developed what is widely known as the Palmgren-Miner or linear cumulative damage theory (Equation 11). Considerable work has been done in attempts to verify this theory, for example the tests by Dolan, Richart and Work (4), Naumann, Hardrath and Guthrie (5) and Naumann and Schott (6). The test results have not all been favorable and, as a result several other theories have been proposed, Freudenthal and Heller (7), Corten and Dolan (8), Valluri (9) and many others. However, the Palmgren-Miner theory probably remains the most widely used theory.

Freudenthal (10) in 1953 introduced the randomized-block type of testing which is an attempt to duplicate actual service stress-time histories. In this type of testing, several stress levels are selected based on service loadings. The specimen is then stressed at each stress level for a certain number of cycles. Each group of cycles at a fixed stress level is referred to as a block. The portion of blocks at each stress level is determined from the service loading and the ordering of the blocks is then randomized. Test results for this type of testing has in general been in close agreement

with the Palmgren-Miner theory (11, p. 288).

Random Fatigue Tests

The random type of stressing which occurs in aircraft structures has been more closely duplicated by the random fatigue tests in which the stress amplitude varies in a completely random manner. Head and Hooke (12) were the first to report tests of this type. Notched cantilever specimens were excited to vibrate at resonance by an electrodynamic shaker driven with a random-noise generator. The resonance provides a narrow band width type of loading, which gives a ratio of the number of zero crossings with positive slope per second, N_0, to the number of positive peaks per second, M, equal to one for the stress history. They found that the Palmgren-Miner theory predicted a lifetime three to three and one-half times greater than that of the test results.

In 1956 McIntosh and Granick (13) vibrated free cantilever specimens at resonance by exciting the fixed end with an electrodynamic shaker driven by a random-noise generator; however, difficulties were encountered with second mode vibrations. In 1961 Smith and Malme (14) used a similar technique and also found that the Palmgren-Miner theory predicted longer lifetimes.

In 1958 Trotter (15) conducted resonant-type random tests of 2024-T3 aluminum alloy and found longer lifetimes at higher rms stress levels and shorter lifetimes at lower levels than

that predicted by the Palmgren-Miner theory.

Fralich (16, 17) tested notched cantilever specimens at resonance using 7075-T6 aluminum alloy in 1959 and 4130 steel in 1961. He found that the Palmgren-Miner theory underestimated the life for the aluminum alloy and overestimated the life for the steel.

Kowalewski (18) in 1959 reported test results on 2024 aluminum alloy. He filtered the random noise input within the range below approximately one-third of the natural frequency of the system. This gave ratios for $N_0/_M$ of 0.98, 0.91 and 0.75. These are apparently the first tests conducted using other than narrow-band type of loading. Kowalewski derived program tests from the random test histories. He found the Palmgren-Miner theory predicted a longer lifetime than that given by the program tests but nearly the same as the random tests when $N_0/_M = 0.98$.

In 1959, Crichlow et al. (19) axially loaded aluminum-sheet specimens with hydraulic servomechanisms controlled by tape recordings of actual aircraft load histories.

In 1963 Swanson (20) tested axially loaded specimens of 2024-T4 aluminum alloy. He used a single-resonant-frequency and also a double-resonant-frequency type of loading, the latter providing a ratio of $N_0/_M$ of 0.577. He found the Palmgren-Miner theory to overestimate the fatigue life by a factor of about three to five for the single-resonant-frequency tests and even more for the two-resonant-frequency type tests.

Fuller (21) in 1963 tested 2024-T3 aluminum alloy using three different power spectrums (see Figure 26) which gave ratios for N_0/M of 0.963, 0.808 and 0.751. He found the Palmgren-Miner theory overestimated the lifetime by a factor of about four and one-half. He found reasonably good agreement with his own theory.

Girks (22), using resonant type random loading, found the Palmgren-Miner theory to give a good estimate of the lifetime for his test results; however, he defined failure when the fatigue crack became a certain length as measured by a 0.2 per cent change in the natural frequency of the specimen.

The Palmgren-Miner theory in general overestimates the fatigue life. The results of Girks suggest that it may be applicable during the crack-initiation and early crack-growth stages. Early failure seems likely since a high stress peak could occur which would cause failure before the crack grew to its expected length.

There does not appear to be any agreement on which of the statistical quantities in the random stress histories are important. For example, Fuller used the average rise between successive positive and negative peaks while the others employed the magnitude of the stress peaks. Also, should the total number of peaks to failure be considered or the total number of zero crossings with positive slope?

DESCRIPTION OF TEST FACILITY

The Iowa State University fatigue testing facility was developed specifically for the purpose of conducting random fatigue tests. The system is discussed in detail in Reference 23.

The end of a small cantilever-beam test specimen is attached through a pinned connection to the moving coil of an electrodynamic shaker. The specimen acts as a spring for the shaker. By utilizing the electrical damping characteristics of the moving coil it was possible to eliminate the resonant behavior of the cantilever-beam specimen. The resulting frequency response is flat from zero out to 220 cycles per second and then falls off. This range includes most of the frequencies encountered in service (24, 25), however, the sound-induced vibrations occurring in rockets are at much higher frequencies.

The input to the system is an electrical signal which could be from a signal generator, strain-gage recording, etc. For the random fatigue tests, a random-noise generator was used. The flat frequency response permits filtering of the random noise input to obtain the desired frequency spectrum of the stress-time history.

Complete System

A schematic of the entire test facility is shown in

Figure 1 and the actual system is shown in Figure 2.

The output from the random-noise generator is filtered to give the desired power spectrum, then amplified with a special transistor power amplifier (26). This amplified signal passes through the moving coil, which is located in the annular air gap of the shaker. The magnetic field in the air gap is provided by the electromagnet of the shaker body. The force generated by the current passing through the moving coil is transmitted to the end of the cantilever specimen through a pinned connection.

The force applied to the end of the specimen is measured with a piezoelectric force transducer located under the upper mounting blocks on the shaker. The transducer output is amplified by a charge amplifier. This signal which is directly proportional to the stress in the specimen is monitored with a true-rms voltmeter and also an oscilloscope. In addition, portions of this signal were recorded on magnetic tape for later analysis. Oscillograph traces were also obtained.

The specimen is connected in series with the coil of the cutoff relay and a six volt power supply. When the specimen breaks, the relay opens and the power to the entire system is cutoff, thus providing shutdown. Fatigue failure was defined as complete fracture of the specimen.

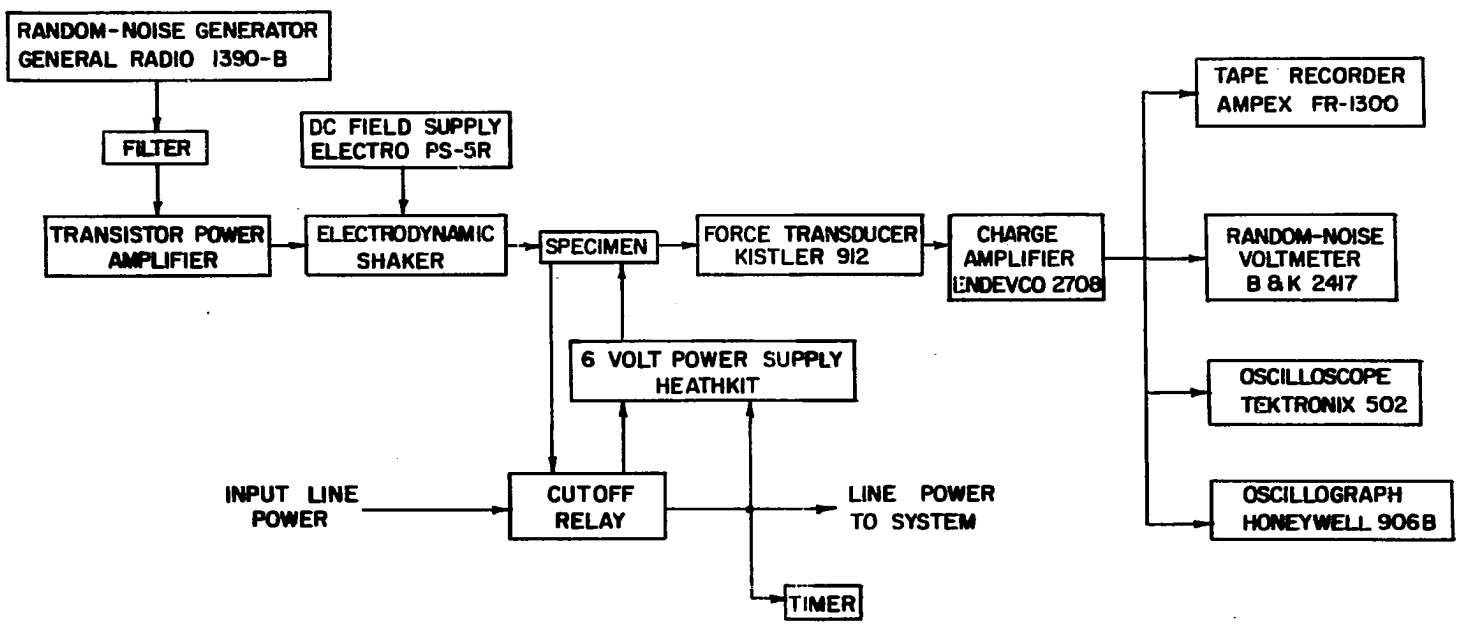

Figure 1. Schematic of fatigue testing facility

Figure 2. Fatigue testing facility

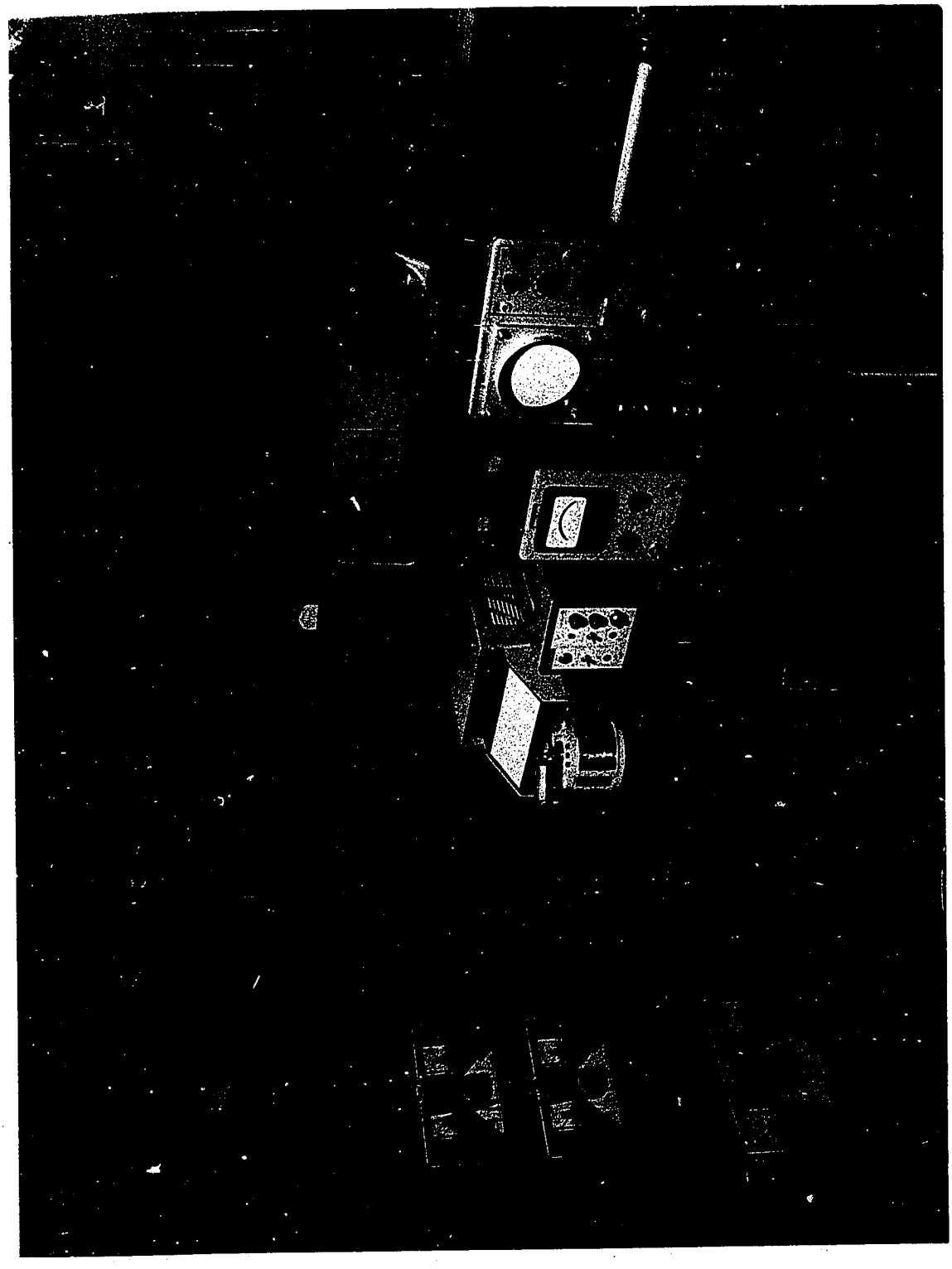

Specimen

The specimens used for this investigation are shown in Figures 3 and 4. Since the spring constant of the specimen affects the frequency response of the system, steel specimens for this test equipment are slightly larger and also thinner than the aluminum specimens.

The tapered portion of the specimen provides a constant stress section. The stress in this section is,

$$\sigma = \frac{6P}{rt^2} , \qquad (1)$$

where

σ = stress on the surface, psi;

P = force applied to the end, lbs.;

r = .204 for this specimen; and

t = specimen thickness, in.

The specimens were cut parallel to the direction of rolling from 13 gage sheets of 2024-T3 aluminum alloy, then machined using a formed milling machine cutter to obtain the tapered section. Each side was ground and then hand polished using successively finer emery paper down to 00 grit (27). The grinding and polishing was all performed in the longitudinal direction of the specimen. The thickness of each specimen was measured and the force required for a specific stress level was determined from Equation 1. The gain of the power amplifier was then adjusted to give this force. The

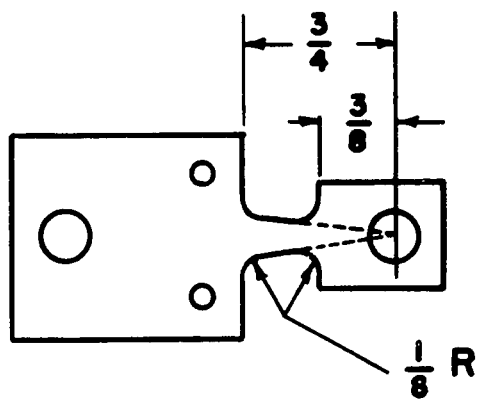

FINAL THICKNESS 0.060 IN.

Figure 3. Aluminum specimen

Figure 4. Aluminum specimen

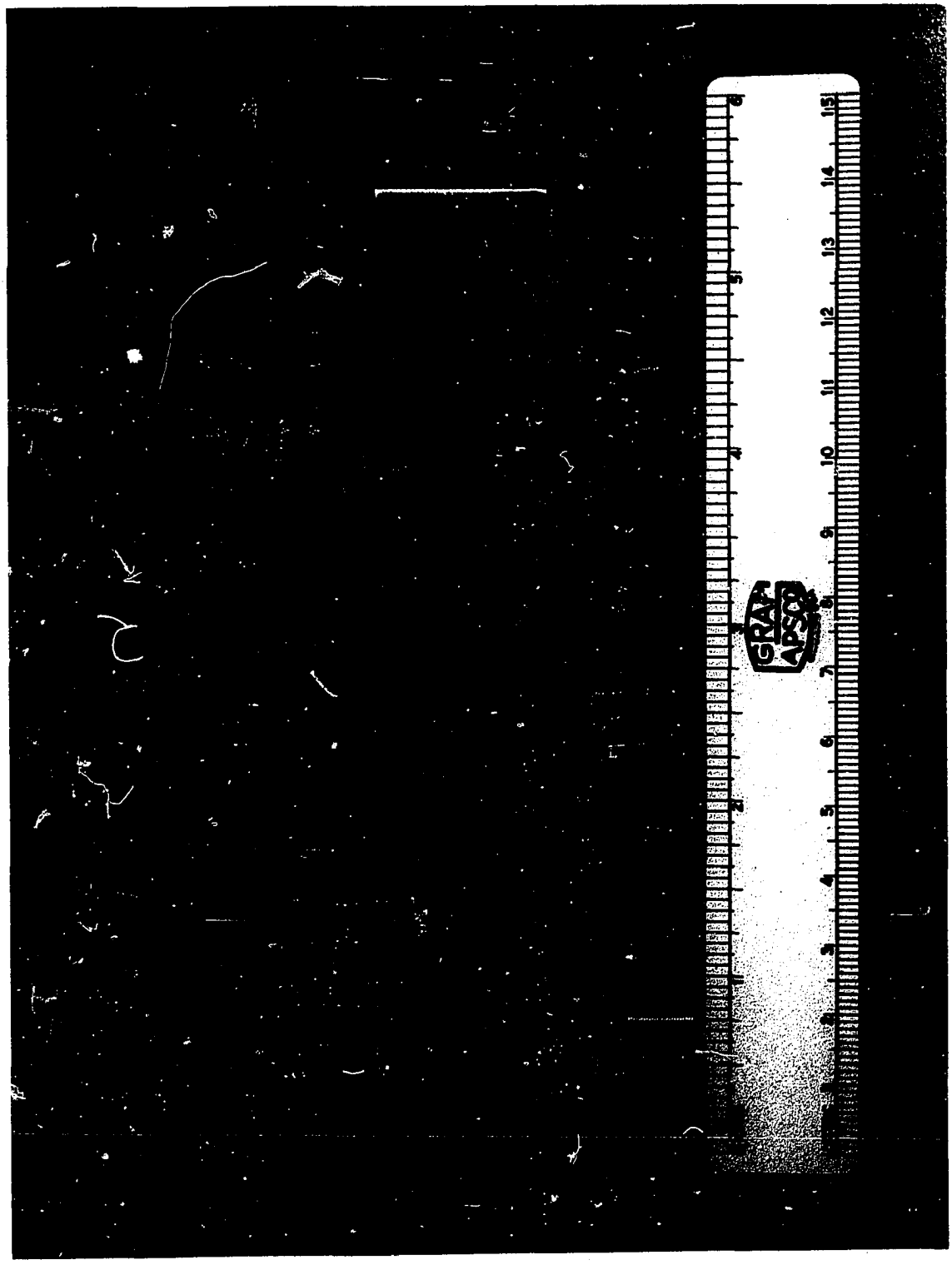

specimens were numbered before being cut from the sheet and then randomized using a table of random numbers.

Electrodynamic Shaker

The electrodynamic shaker is shown in Figures 5 and 6. A pinned connection is used at the specimen so that a bending moment is not applied to the end of the specimen. This linkage along with the mounting blocks are machined from non-magnetic stainless steel, except for the hardened steel pin.

Cooling for the moving coil is provided by drawing air down through the annular air gap.

Force Transducer

The Kistler Model 912 piezoelectric force transducer is also illustrated in Figures 5 and 6. The transducer acts as one point of the two point support for the upper mounting block. The second support eliminates the application of a bending moment to the transducer. The force on the transducer is directly proportional to the force applied to the end of the specimen. This was verified by static and dynamic calibration of the transducer using strain gages mounted on one of the specimens.

Since the spring constant of the transducer is very large, there is no noticeable vibration of the upper mounting block.

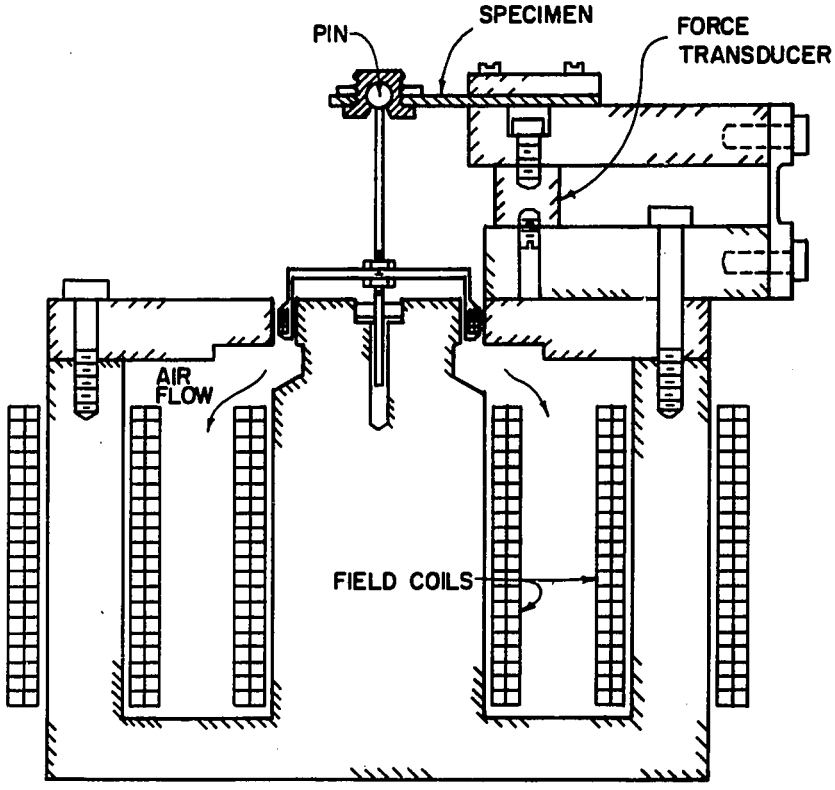

Figure 5. Cross-section of electrodynamic shaker

Figure 6. Electrodynamic shaker

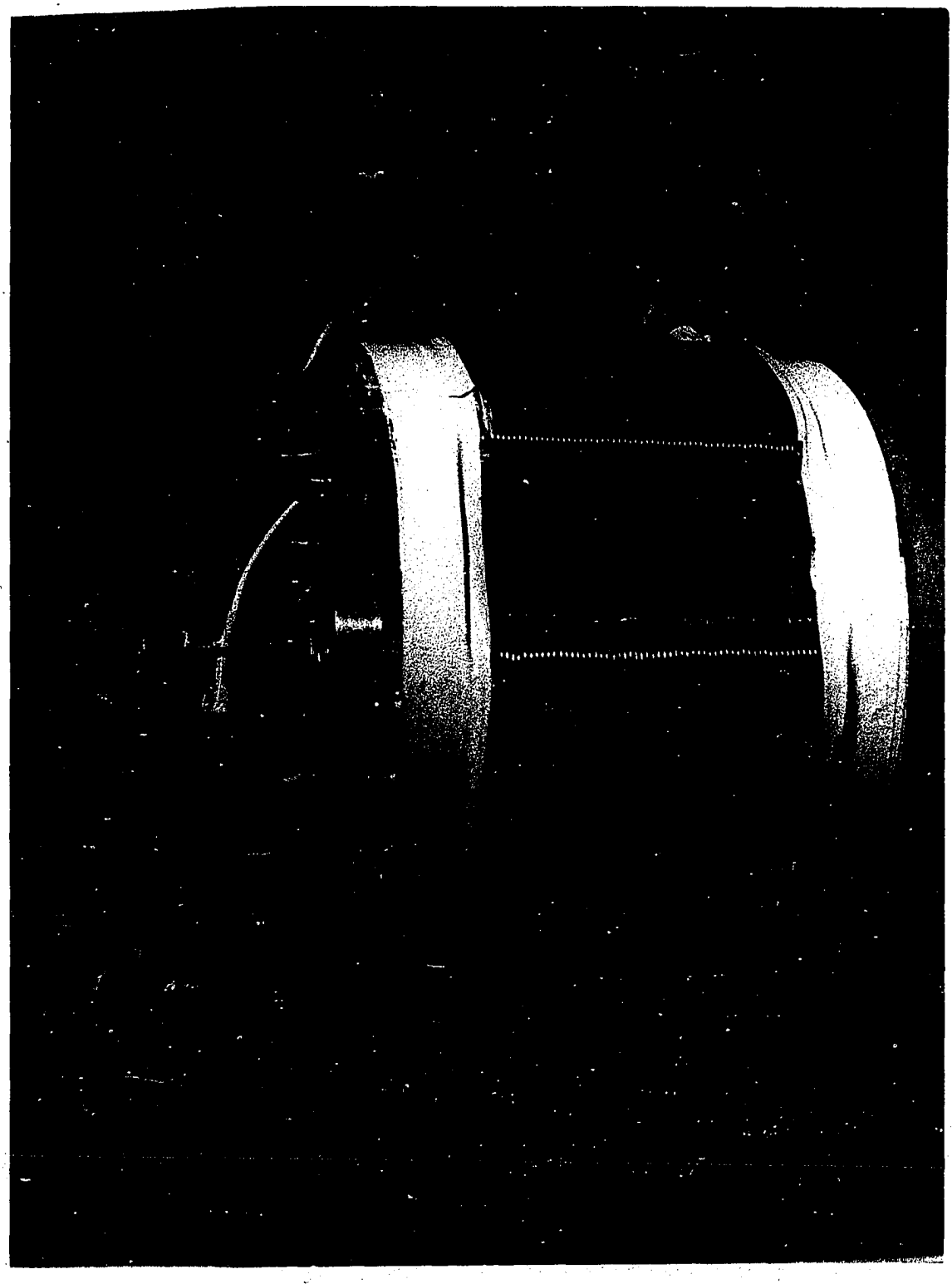

Filters

For a linear system excited by a noise input, the power spectral density function of the output, $G(\omega)$, is (28, p. 337)

$$G(\omega) = \left|Y(j\omega)\right|^2 G_n(\omega) \qquad (2)$$

where

$Y(j\omega)$ = transfer function of the system, and

$G_n(\omega)$ = power spectral density function of the input noise.

For white noise $G_n(\omega)$ equals a constant and, therefore, the power spectral density curve of the output will be a constant times the square of the frequency response curve. The frequency response of the shaker is flat from 0 to 220 cycles per second and the output of the random-noise generator has a flat power spectrum from 15 to 20,000 cycles per second (29). Therefore, the power spectrum of the stress generated in the specimen will have the same shape as the frequency response of the filter for frequencies between 15 and 220 cycles per second.

Active filters were made using a Heath Model EUW-19 operational amplifier unit.

Broad-band filter

For the broad-band random fatigue tests, it was desired to have a flat power spectrum over as wide a frequency range

as possible and with as sharp of cutoffs as possible. An active band-pass filter was made using the method described by Hansen (30).

The circuit diagram for the filter is shown in Figure 7 and the frequency response of the overall system when using this filter is shown in Figure 9.

Narrow-band filter

The narrow-band filter was made by placing a rejection filter in the feedback loop of an operational amplifier. The circuit diagram is shown in Figure 8 and the frequency response of the system using this filter is also shown in Figure 9.

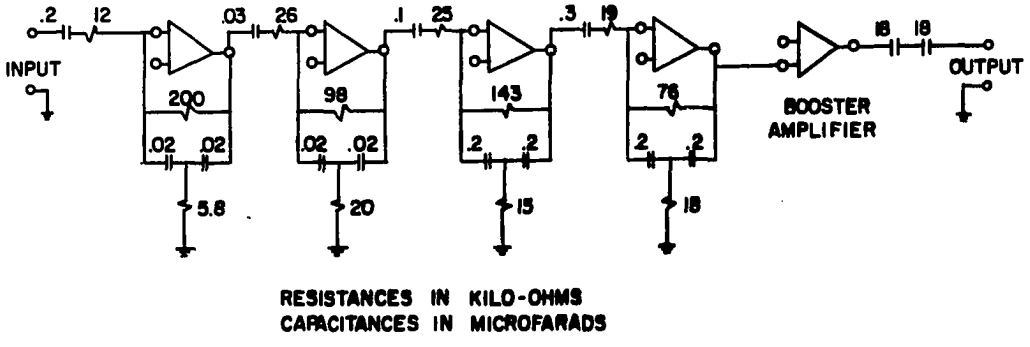

Figure 7. Broad-band filter

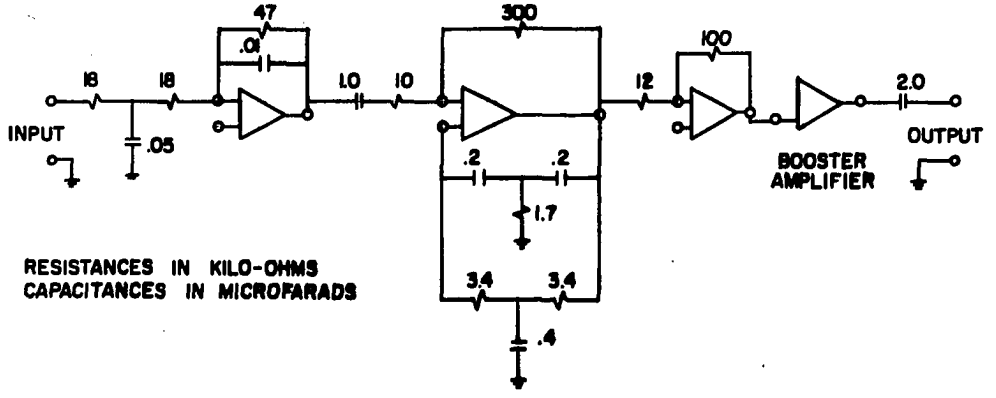

Figure 8. Narrow-band filter

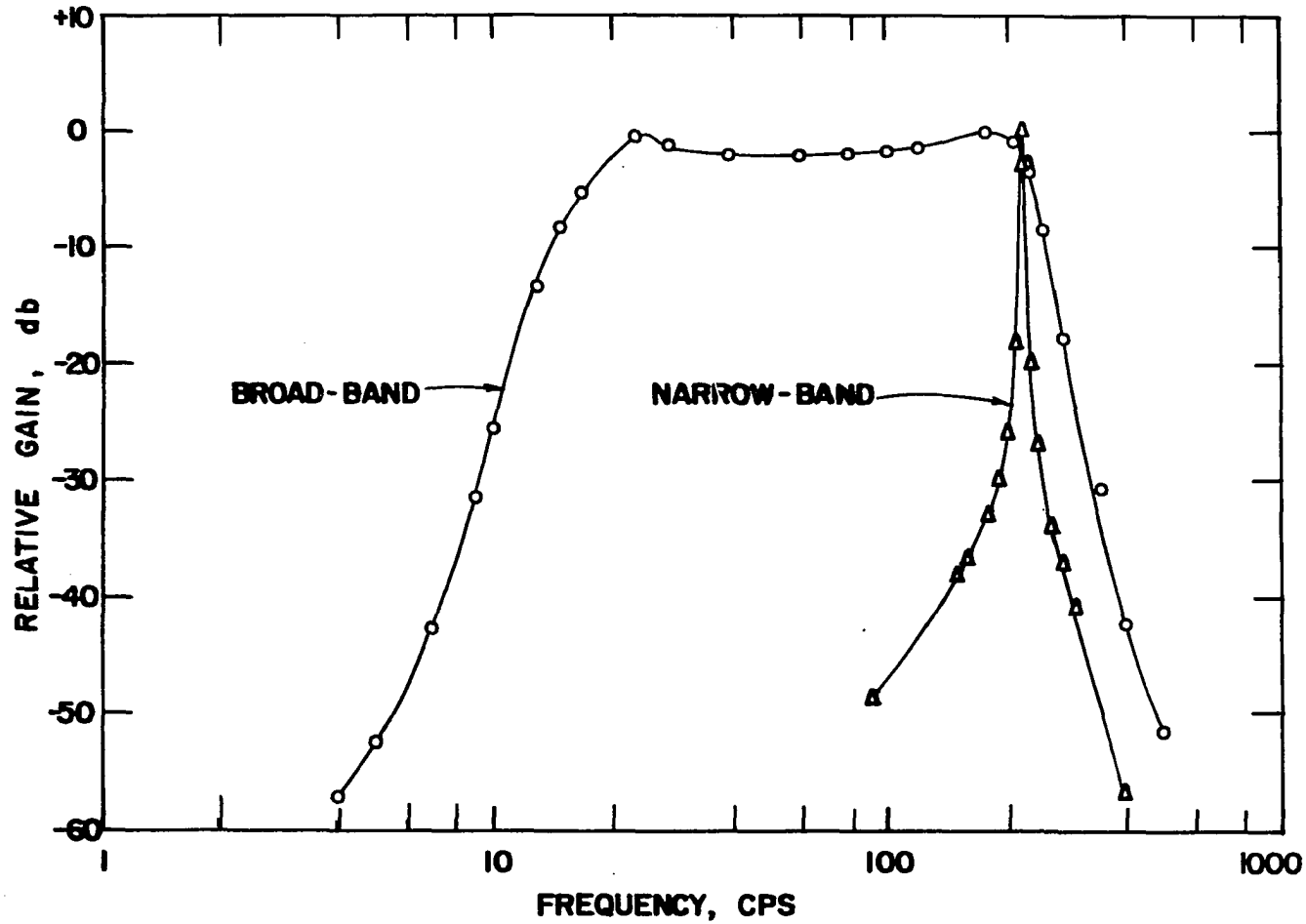

Figure 9. Frequency response of complete system

DESCRIPTION OF RANDOM FATIGUE TESTS

Gaussian Noise

A Gaussian signal is defined as a signal whose statistical characteristics are described by normal probability densities (28, p. 332). The output signal from the General Radio Random-Noise Generator (type 1390-B) has been found to be very close to Gaussian when comparing the first probability density function (29).

Power Spectral Density

In order to determine the effect of frequency bandwidth on the fatigue behavior under random loading, tests were conducted using a very narrow-pass filter, which produces a narrow spectrum, and using a band-pass filter which gives a wider spectrum.

As mentioned previously, the power spectral density is equal to a constant times the square of the frequency response of the system. The resulting spectrums are compared with the measured spectrums in Figure 10 for the broad-band loading and in Figure 11 for the narrow-band loading. The power spectrums were measured from magnetic-tape recordings by Collins Radio Company, Cedar Rapids, Iowa.

The frequency response curve shown in Figure 9 for the broad-band loading is flat within 2db; however, the resulting power spectral density curve shown in Figure 10 does not

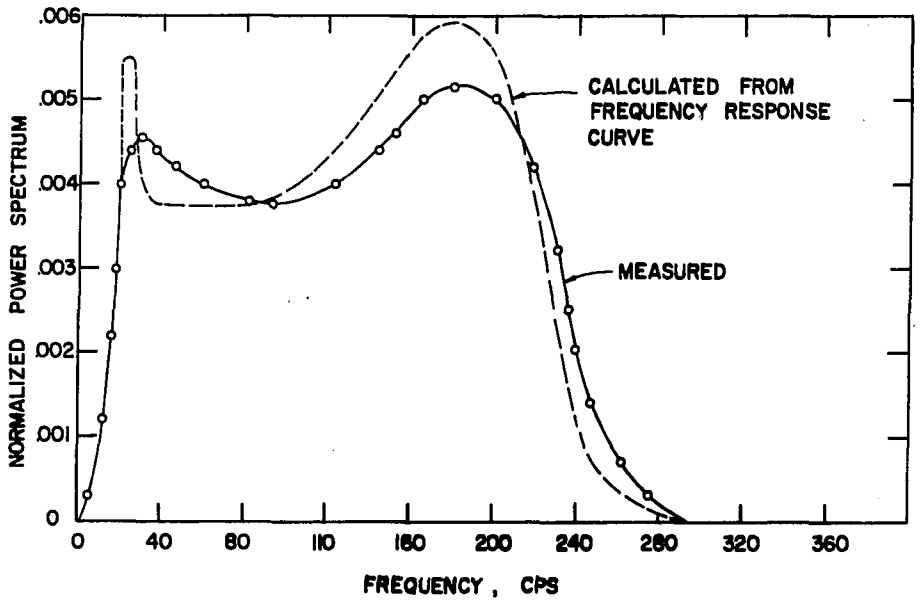

Figure 10. Normalized power spectrum for broad-band loading

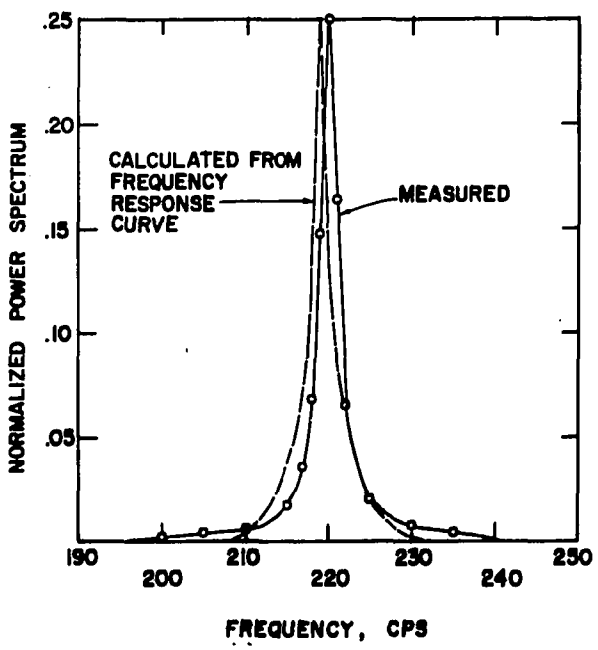

Figure 11. Normalized power spectrum for narrow-band loading

appear as flat because of the logarithmic vertical scale used in Figure 9 and the linear vertical scale in Figure 10. Further deviation results from squaring the frequency response to obtain the power spectrum. Had this been realized at the time, a greater effort would have been made to obtain a flatter curve for the broad-band filter.

The stress-time histories for the two types of loading are illustrated by the oscillograph traces shown in Figures 12 and 13.

Ratio of Zero Crossings with Positive Slope Per Second to Positive Peaks Per Second

The ratio of the number of zero crossings with positive slope per second to the number of positive peaks per second has been used to express the type of stress-time history for random loading.

For a stationary Gaussian signal with zero mean, the expected number of zero crossings with positive slope per second, N_0, is

$$N_0 = \frac{1}{2\pi}\left[\frac{\int_0^\infty (2\pi f)^2 G(f)\,df}{\int_0^\infty G(f)\,df}\right]^{\frac{1}{2}}, \qquad (3)$$

Figure 12. Oscillograph trace of stress-time history for narrow-band loading

Figure 13. Oscillograph trace of stress-time history for broad-band loading

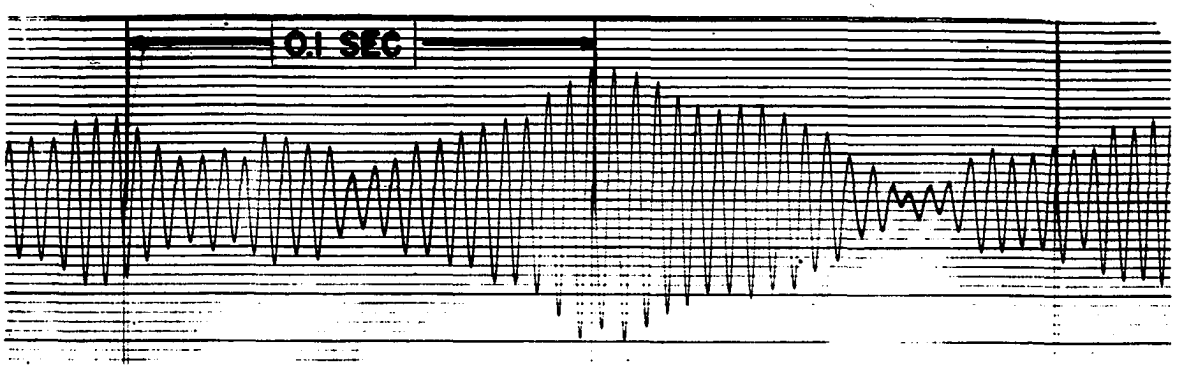
0.1 SEC

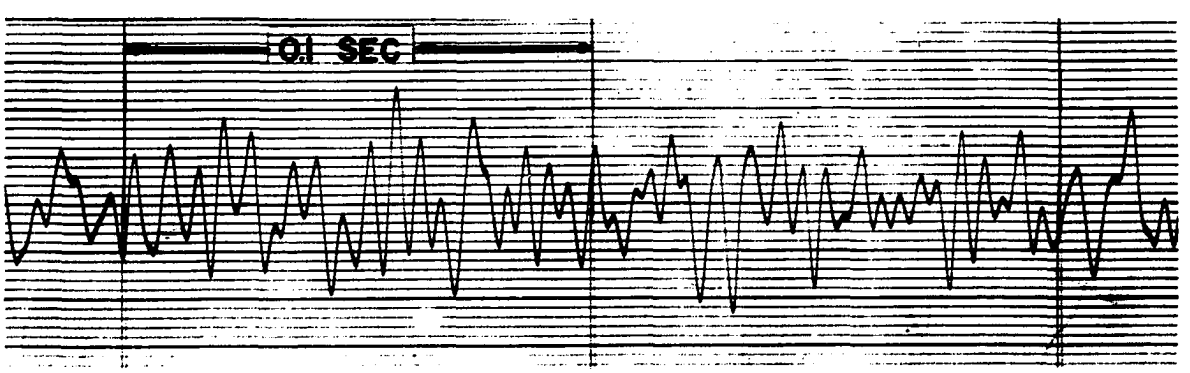
0.1 SEC

where

$G(f)$ = power spectral density and

f = frequency, cps.

The expected number of positive peaks per second, M, is

$$M = \frac{1}{2\pi}\left[\frac{\int_0^\infty (2\pi f)^4 G(f)\,df}{\int_0^\infty (2\pi f)^2 G(f)\,df}\right]^{\frac{1}{2}} \tag{4}$$

These results were first derived by Rice (31, pp. 73-75) and are also given by Bendat (32, p. 38).

The desired ratio is then N_0/M. For the broad band loading, this ratio was calculated by approximating the power spectrum as follows:

$$G(f) = \frac{af^6}{(16)^5} \quad \text{for} \quad 0 < f \leq 16 \ ,$$

$$= a \quad \text{for} \quad 16 < f \leq 220 \ , \text{ and}$$

$$= \frac{a(220)^8}{f^8} \quad \text{for} \quad 220 < f < \infty \ .$$

The calculated values of N_0 and M are compared with the measured values in Table 1 for the broad-band loading. The

Table 1. Number of zero-crossings with positive slope per second and number of positive peaks per second for broad-band loading

	Calculated	Measured
Number of zero-crossings with positive slope per second, N_0	154.7	153.6
Number of positive peaks per second, M	220	195
N_0/M	.703	.788

measured values were obtained by manually counting N_0 and M on the oscillograph traces for a one second duration period and averaging the values from eight to ten traces. There was little variation between traces taken at different periods during a single test or between different tests at the same or different stress levels.

For the narrow-band loading, the ratio N_0/M was not calculated because of the very narrow bandwidth (down 3db one cycle per second on each side of the 219 cycles-per-second center frequency). For all of the oscillograph traces observed, there was always a zero crossing between any two successive positive and negative peaks and, therefore, $N_0/M = 1$.

Peak Probability Density Function

The stress peaks which occur during the time history are used later for predicting the fatigue life. The peak

probability density function, W(z), defines the probability that a positive peak will fall between z and z + dz. For a stationary Gaussian process, this is expressed by the formula (32, p. 39),

$$W(z) = \frac{K_1}{\sqrt{2\pi}} e^{-z^2/2K_1^2} + \left(\frac{N_0}{M}\right) z e^{-z^2/2} \left[1 - P\left(\frac{z}{K_2}\right)\right] , \qquad (6)$$

where

$$K_1 = \sqrt{1 - \left(\frac{N_0}{M}\right)^2} ,$$

$$K_2 = \frac{K_1}{\left(\frac{N_0}{M}\right)} , \text{ and}$$

$$P\left(\frac{z}{K_2}\right) = \frac{1}{\sqrt{2\pi}} \int_{z/K_2}^{\infty} e^{-y^2/2} \, dy .$$

$P(z/K_2)$ is the probability for a normal distribution with zero mean and unit variance that the value z/K_2 will be exceeded. The value of this integral is readily available in statistical tables. Equation 6 for W(z) is in terms of the normalized variable z with zero mean and unit variance.

The shape of W(z) depends on the ratio N_0/M, which is always between zero and one:

$$0 \leq \frac{N_0}{M} \leq 1 \quad .$$

When $N_0/M = 0$, Equation 6 reduces to

$$W(z) = \frac{1}{\sqrt{2\pi}} e^{-z^2/2} \quad , \tag{7}$$

which is the normal probability density function.

When $N_0/M = 1$, Equation 6 becomes,

$$W(z) = ze^{-z^2/2} \quad , \tag{8}$$

which is the Rayleigh probability density function.

For very narrow bandwidths, N_0/M approaches unity and Equation 8 applies. When the bandwidth becomes infinitely wide, $N_0/M = 0$ and the probability density function is normal as given by Equation 7.

Figure 14 shows the Rayleigh probability density function along with the histogram for the narrow-band fatigue tests. The histogram was obtained from the tape recordings using a peak-level counter which was made available by Collins Radio Company.

For the broad-band random fatigue tests, $N_0/M = .788$. The peak probability density function for this ratio of N_0/M is shown in Figure 15 along with the experimentally determined histogram. The histogram for this case was obtained from the oscillograph traces by manually counting the number of peaks

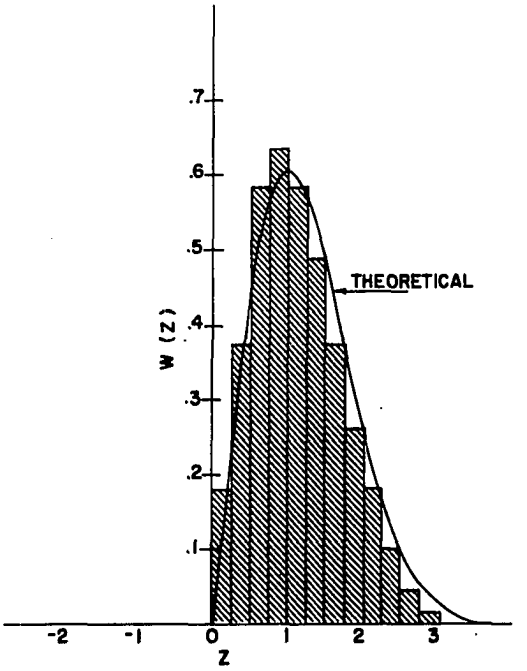

Figure 14. Normalized peak probability density function for narrow-band loading (Rayleigh)

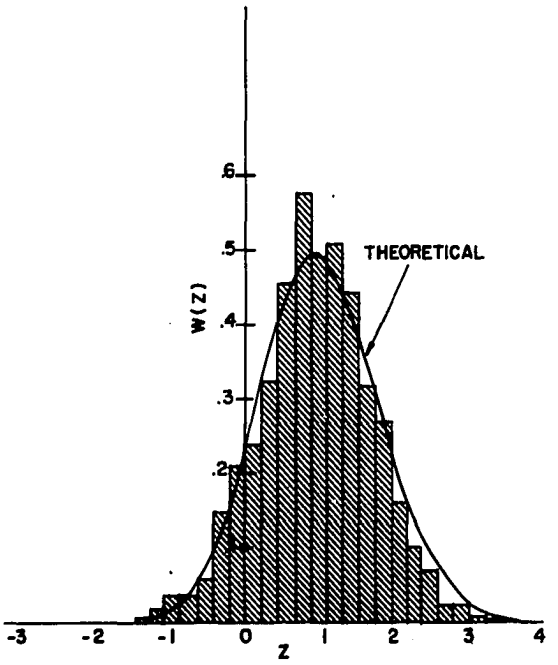

Figure 15. Normalized peak probability density function for broad-band loading

occurring at the different stress levels.

Note that the peak probability density function, W(z), depends only on the ratio N_0/M, but N_0/M is a function of the shape of the power spectrum.

In terms of the normalized variable, z, the expected value of z^b is,

$$E(z^b) = \int_{-\infty}^{\infty} z^b W(z)\,dz \quad , \tag{9}$$

which is of interest later in predicting the fatigue life.

TEST RESULTS

Constant-Amplitude, Sine-Wave Fatigue Tests

The constant-amplitude, sine-wave test results are shown in Figure 16 with log σ plotted against log N. The data points represent the logarithmic average of five samples tested at each stress level and the tick marks show the scatter band.

The straight line portion of this curve can be represented by the equation,

$$N\sigma^{b} = B \quad , \tag{10}$$

where

$b = 7.1$ and

$B = 4.68 \times 10^{16}$.

Corten-Dolan Constant

Seven two-level, sine-wave tests were run to determine the constant, d, for the Corten-Dolan theory. The value of d was determined by substituting the test results into Equation 22. The results are shown in Table 2. Corten and Dolan found d to be approximately equal to 0.85 times b, which for this case would be 6.03. This is in close agreement with the average value of 5.89.

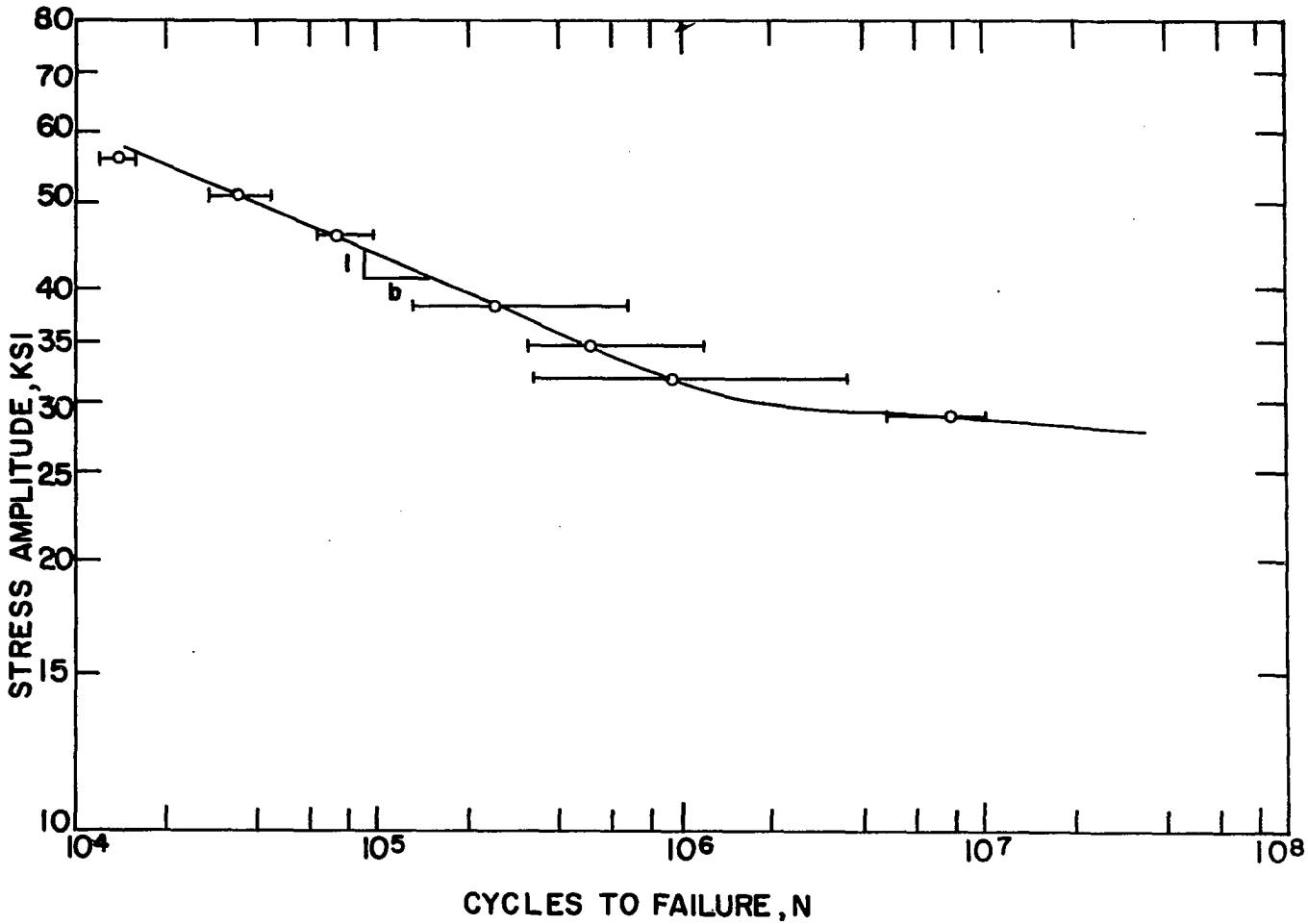

Figure 16. Constant-amplitude, sine-wave fatigue test results

Table 2. Test results for determining the Corten-Dolan constant, d

σ_1	N_1	σ_2	N_g	d
38.8	91,200	29.6	906,000	7.71
38.8	68,416	29.6	638,504	5.65
38.8	49,042	29.6	705,740	5.62
38.8	48,110	29.6	402,319	3.31
38.8	60,047	29.6	629,656	5.39
38.8	54,034	29.6	602,169	5.18
38.8	60,038	29.6	1,347,333	8.38
				Average = 5.89

Random Fatigue Tests

The results of the random fatigue tests are shown in Figure 17 which is a plot of log σ_{rms} versus log N_p, where N_p is the total number of positive peaks to failure. For each type of loading, seven samples were tested at the highest stress level and ten samples were tested at each of the remaining four stress levels. The number of peaks to failure was assumed to have a logarithmic-normal distribution. A sample size of ten is considered too small to apply the Chi-Square goodness-of-fit test to check this assumption; therefore, a check was made by plotting the variation on probability paper. This is shown in Figures 18 and 19 for the broad-band and narrow-band test results respectively. A straight line on

this plot represents a normal distribution.

In Figure 17, the data points represent the logarithmic-average and the tick marks indicate the scatter. The negative slope of each of the random fatigue curves is 1/5.7 as compared to 1/7.1 for the constant-amplitude, sine-wave curve, which is also shown in Figure 17.

It is surprising that the lifetime was not much shorter at the high stress level since the loading contained peak forces which would produce stresses in the order of 90,000 psi according to the elastic beam formula, Equation 1. The tensile strength and yield strength for the material were 70,900 psi and 51,300 psi, respectively (33); therefore, the material was stressed well into the plastic region. According to the theoretical peak probability density curves, Figures 14 and 15, the percentage of peaks which exceeded the yield strength for each stress level is given below. The material

Table 3. Percent of positive peaks greater than the yield strength

σ_{rms}	Narrow-band	Broad-band
26.4	14.6	11.5
22.7	7.4	6.0
17.0	0.9	0.7
13.2	-	-
11.3	-	-

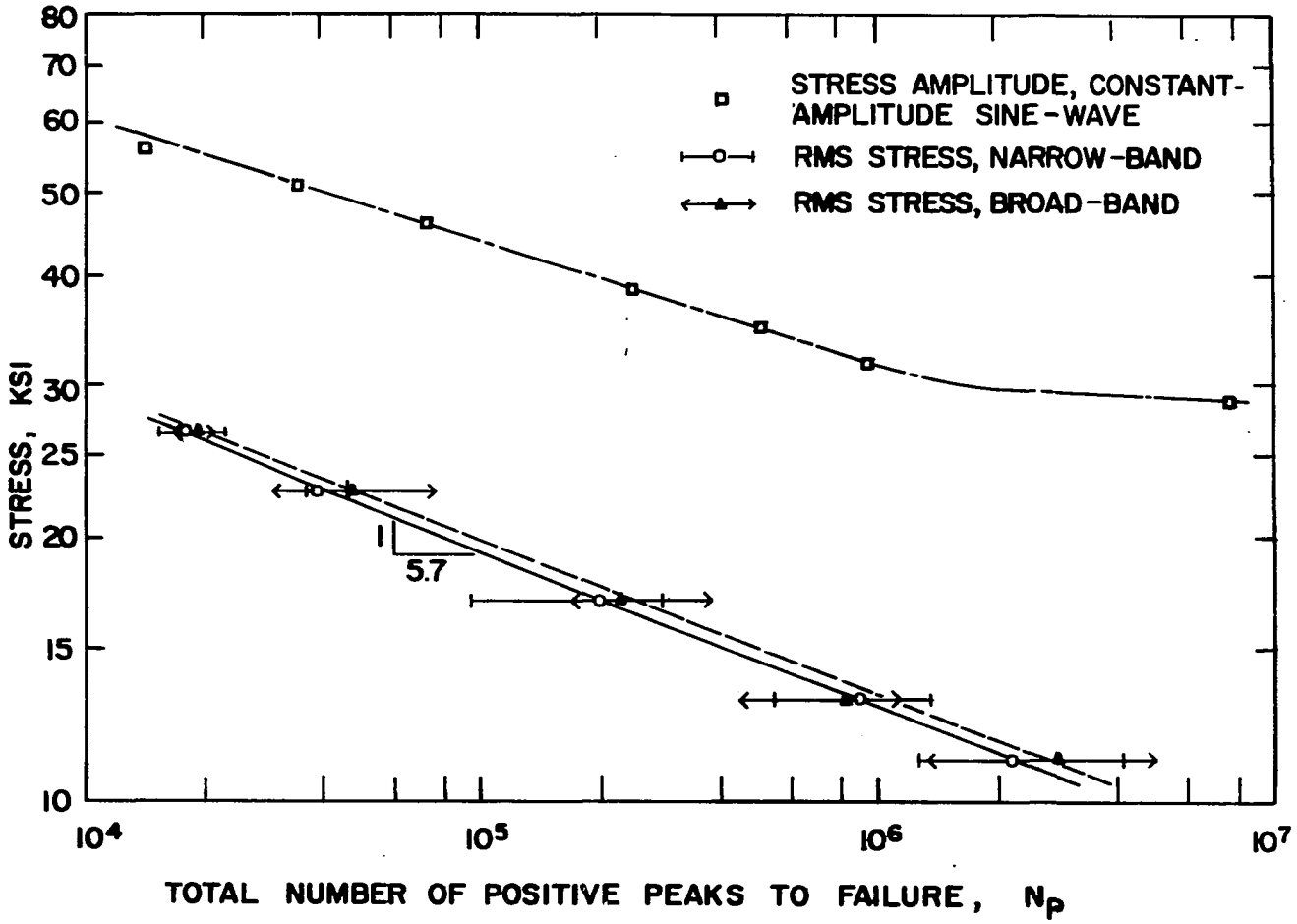

Figure 17. Random fatigue test results

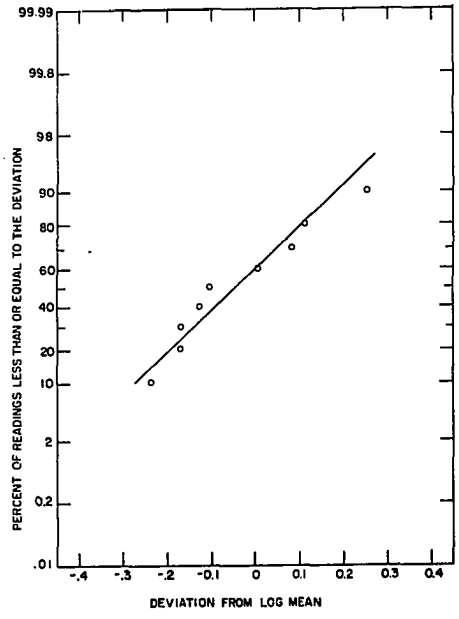

Figure 18. Test of logarithmic-normal distribution for N_p—narrow-band loading, σ_{rms} = 11.3 ksi

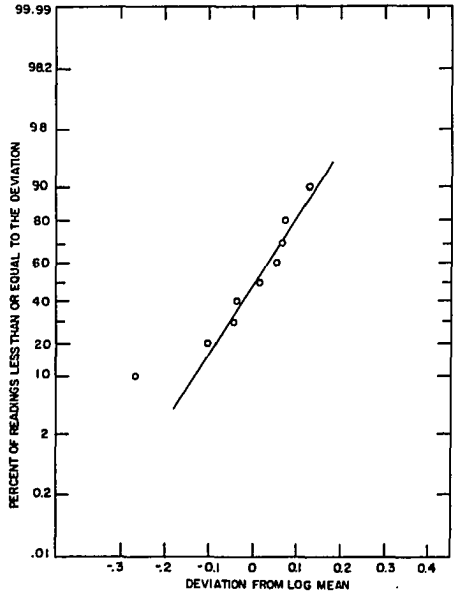

Figure 19. Test of logarithmic-normal distribution for N_p—broad-band loading, σ_{rms} = 13.2 ksi

apparently is strain hardened by those stress peaks which exceed the yield strength. This increases the fatigue life. Also, this overstraining may be causing residual compressive stresses. These would reduce the fatigue damage caused by the stress peaks below the yield strength. This would account for the longer than expected lifetimes at the higher stress levels, and also would explain why the random fatigue curves have a steeper slope than the constant-amplitude curve.

PREDICTED FATIGUE LIFE

Palmgren-Miner Theory

According to the Palmgren-Miner theory (2, 3), the damage to the material caused by n cycles of stress amplitude σ is n/N, where N is the fatigue life at stress amplitude σ as given by the constant-amplitude, sine-wave fatigue curve. Furthermore, the fractional damage occurring at this stress level is added to the corresponding damages occurring at other stress levels. Failure is assumed to occur when this total damage, D, is equal to one. D is also known as the cumulative cycle ratio and is given by the formula,

$$D = \sum_{i=1}^{j} \frac{n_i}{N_i} , \qquad (11)$$

where j refers to the number of distinct stress levels.

The value of D has been found experimentally to vary considerably from the value of one as suggested by Palmgren and Miner; however, the theory is still widely used because of its simplicity and also because of insufficient test data to verify some of the other cumulative damage rules. The order in which the stress levels are applied is not taken into account by the theory; however, it does affect the value of D. For example, in two-level sine-wave tests on steel specimens, if $\sigma_1 < \sigma_2$, then $D > 1$, and if $\sigma_1 > \sigma_2$, then $D < 1$ (34, p. 117). These results are not as consistent for aluminum alloys.

In addition, it has been found that when the stress at each level is applied a few cycles at a time, with stress levels being repeated, the value of D is closer to unity (35). Thus, D may be expected to have a value very close to unity for random stress histories.

The Palmgren-Miner theory can be extended to random loading by assuming that the damage caused by each positive stress peak is the same as the damage caused by one cycle in a sine wave test of the same stress amplitude (36, p. 115). Let N_p be the total number of positive peaks to failure. The expected number of peaks, $n(\sigma)$, occurring between σ and $\sigma + d\sigma$ is then

$$n(\sigma) = N_p W(\sigma) d\sigma \ , \tag{12}$$

where $W(\sigma)$ is the peak probability density function. According to the Palmgren-Miner theory, a single stress peak of amplitude σ causes a damage of $1/N(\sigma)$, where $N(\sigma)$ is the fatigue life at stress level σ in the constant-amplitude fatigue test. The expected damage for all positive peaks occurring between σ and $\sigma + d\sigma$ is then,

$$\frac{n(\sigma)}{N(\sigma)} = \frac{N_p W(\sigma) d\sigma}{N(\sigma)} \ . \tag{13}$$

The total expected damage, E(D), is the sum of all the incremental damages given by Equation 13. This sum is

$$E(D) = N_p \int_{-\infty}^{\infty} \frac{W(\sigma)}{N(\sigma)} d\sigma \quad . \tag{14}$$

If there be no limit to the maximum stress which can occur during the entire stress history, then the value of N from Equation 10 can be substituted into Equation 13 for $N(\sigma)$, which gives,

$$E(D) = \frac{N_p}{B} \int_{-\infty}^{\infty} \sigma^b W(\sigma) d\sigma \quad . \tag{15}$$

Noting that the integral in Equation 15 is the expected value of the stress peaks raised to the b power, $E(\sigma_p^b)$, and assuming $E(D) = 1$, then Equation 15 can be written,

$$N_p E(\sigma_p^b) = B \quad , \tag{16}$$

which is of the same form as Equation 14.

In terms of the normalized peak probability density function, W(z), Equation 15 becomes,

$$E(D) = \frac{N_p \sigma_{rms}^b}{B} \int_{-\infty}^{\infty} z^b W(z) dz \quad , \tag{17}$$

where σ_{rms} is the root-mean-square value of the instantaneous stress and not of the stress peaks.

When a mean compressive stress along with a fluctuating stress is applied to a material such that the stress always remains compressive, no fatigue failure will occur (34, p. 104). This indicates that only the positive peaks occurring above zero will contribute to the fatigue damage. The total number of these peaks is

$$N_{p>0} = N_p \int_0^\infty W(z)dz \quad , \tag{18}$$

and Equation 17 becomes

$$E(D) = \left[N_p \int_0^\infty W(z)dz \right] \frac{\sigma_{rms}^b \int_0^\infty z^b W(z)dz}{B \int_0^\infty W(z)dz} \quad , \tag{19}$$

which reduces to

$$E(D) = \frac{N_p \sigma_{rms}^b}{B} \int_0^\infty z^b W(z)dz \quad . \tag{20}$$

The integral in the denominator of Equation 19 is required to normalize the new peak probability density function which is for only the stress peaks occurring above zero.

The peak probability density function, W(z), is given by Equation 6. The method used to evaluate $\int_0^\infty z^b W(z)dz$ is discussed in the Appendix.

For the test results, the expected value of the damage according to Equation 20 is given in Table 4. According to

Table 4. Expected value of fatigue damage—Palmgren-Miner theory

σ_{rms}	Narrow-band E(D)	Broad-band E(D)
26.4	.710	.599
22.7	.474	.482
17.0	.337	.306
13.2	.254	.184
11.3	.205	.210

the Palmgren-Miner theory, failure will occur when E(D) = 1.0; however, it is seen that failure occurred prior to this. Letting E(D) = 1.0 in Equation 20 gives,

$$N_p = \frac{B}{\sigma_{rms}^b \int_0^\infty z^b W(z)dz} , \qquad (21)$$

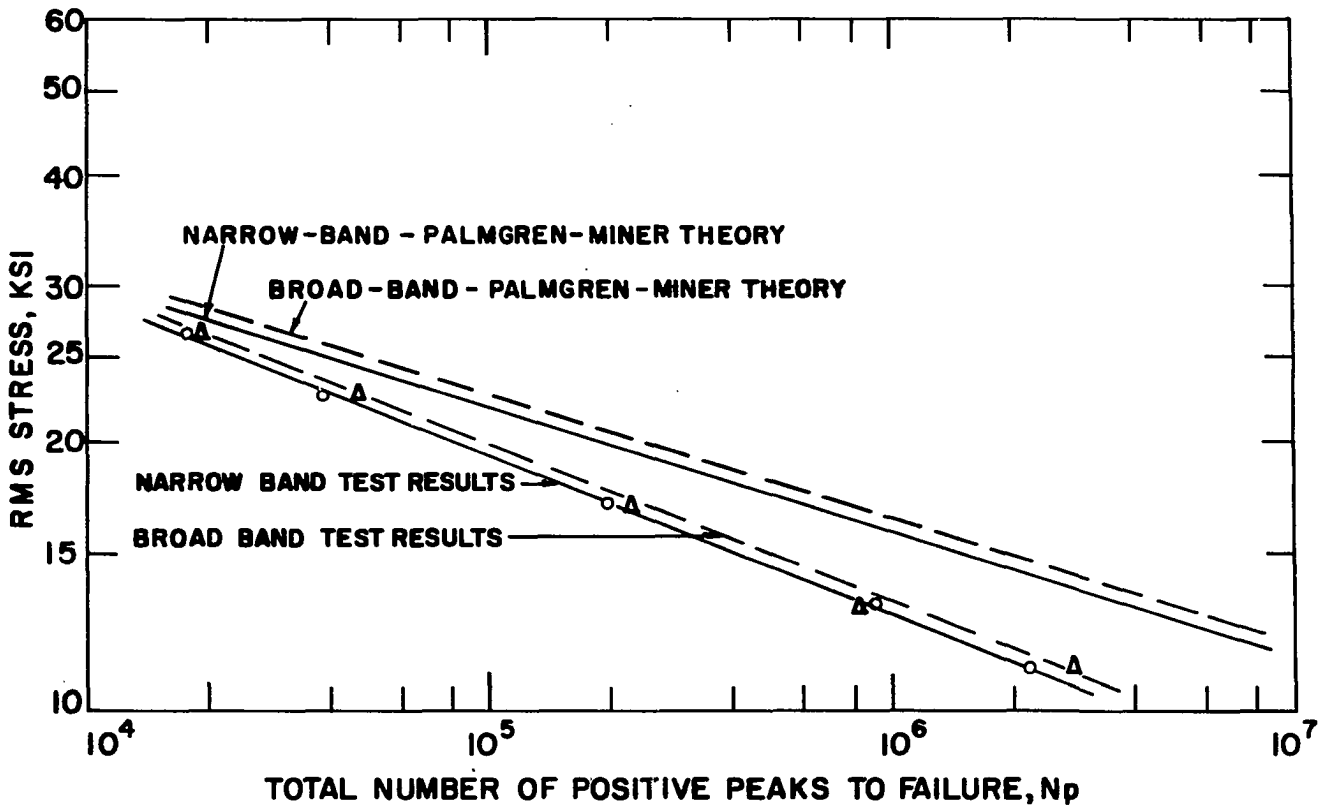

Figure 20. Predicted fatigue life from Palmgren-Miner theory

which is the fatigue curve for the Palmgren-Miner theory. This is shown in Figure 20 for both the narrow-band and broad-band loading. According to Equation 21, the random fatigue curve should be parallel to the constant-amplitude, sine-wave fatigue curve for both types of random loading.

Corten-Dolan Theory

Corten and Dolan (8) based their theory of cumulative damage on the number of damage nuclei formed, which were assumed to be caused by the highest stress level, and on the rate at which the fatigue crack propagates.

The Corten-Dolan equation for sine-wave loading is

$$N_g = \frac{N_1}{\sum_{i=1}^{j} \alpha_i \left(\frac{\sigma_i}{\sigma_1}\right)^d} , \qquad (22)$$

where

N_g = total number of cycles to failure,

α_i = percentage of cycles at stress σ_i,

d = material constant,

σ_1 = stress amplitude of largest stress applied, and

N_1 = fatigue life at stress σ_1.

This equation can be reduced to a Palmgren-Miner type summation on the modified log σ-log N curve shown in Figure 21

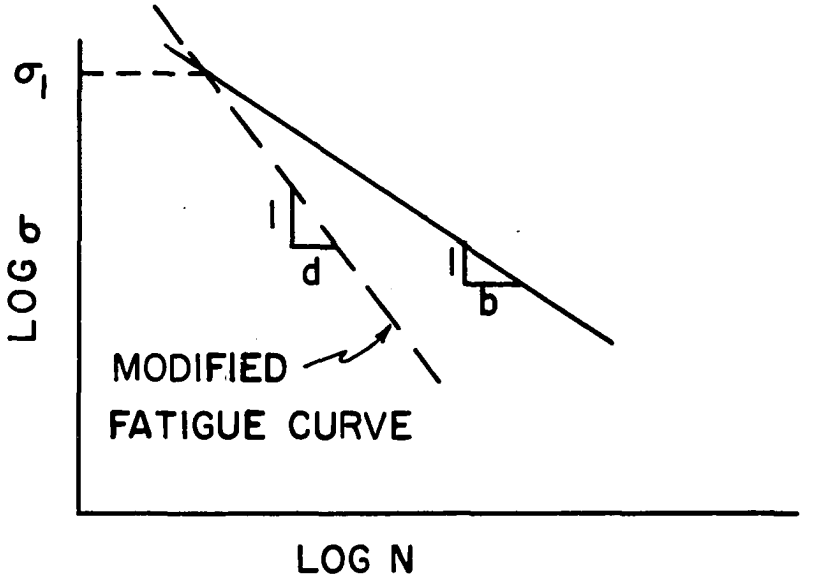

Figure 21. Modified fatigue curve for Corten-Dolan theory

(37). The equation of this curve is

$$N'\sigma^{d} = A \quad , \tag{23}$$

where A and d are constants. If α_i is the portion of cycles at stress amplitude σ_i, then

$$\alpha_i = \frac{n_i}{N_g} \tag{24}$$

where n_i is the number of cycles at σ_i. Substituting Equation 24 into Equation 22 and rearranging gives,

$$\sum_{i=1}^{j} n_i \left(\frac{\sigma_i}{\sigma_1}\right)^{d} = N_1 \quad . \tag{25}$$

From Equation 23,

$$\sigma_1^{d} = \frac{A}{N_1'} \quad , \tag{26}$$

and

$$\sigma_i^{d} = \frac{A}{N_i'} \quad . \tag{27}$$

Substituting Equations 26 and 27 into Equation 25 gives

$$\sum_{i=1}^{j} \frac{n_i}{N_i'} = 1 \quad , \tag{28}$$

which is the Palmgren-Miner type summation on the modified fatigue curve.

With the Corten-Dolan theory in this form, it can be

extended to random loading in the same manner that the Palmgren-Miner rule was extended in arriving at Equation 20. This gives for the Corten-Dolan theory,

$$N_p = \frac{A}{\sigma_{rms}^d \int_0^\infty z^d W(z)\,dz} \quad . \tag{29}$$

Corten and Dolan found the value of d to be constant for different values of the maximum stress, σ_1. Therefore, the constant A must change with changing values of σ_1, since the modified fatigue curve intersects the regular fatigue curve at σ_1.

For random loading, the probability that one peak out of an interval of m peaks will be equal to or exceed the stress level σ_1' is

$$\frac{1}{m} = \int_{z_1'}^\infty W(z)\,dz \quad , \tag{30}$$

where

$$z_1' = \sigma_1' / \sigma_{rms} \quad .$$

If m is large, it can be assumed that the largest stress peak which occurs during the interval is nearly equal to σ_1'. Therefore, σ_1 in the Corten-Dolan theory is set equal to σ_1'. Since the modified fatigue curve intersects the regular

fatigue curve at this stress level,

$$A = (\sigma_{rms} z_1')^{d-b} B \quad . \tag{31}$$

Substituting this into Equation 29 gives

$$N_p = \frac{B}{(z_1')^{b-d} \sigma_{rms}^b \int_0^\infty z^d W(z)\,dz} \quad . \tag{32}$$

Comparing this with Equation 21 shows that for a given type of random loading, the Corten-Dolan theory differs from the Palmgren-Miner theory only by a constant, since $(z_1')^{b-d}$, B and each of the integrals will be constant for any rms stress level if m is constant. Also, the random fatigue curves, log σ_{rms} versus log N_p, defined by these two equations will be parallel and, in addition, parallel to the constant-amplitude, sine-wave fatigue curve.

If the damage, D_i, caused by n_i cycles is given by

$$D_i = \frac{n_i}{N_i'} \quad , \tag{33}$$

then the expected value of the damage E(D), becomes

$$E(D) = \frac{N_p (z_1')^{b-d} \sigma_{rms}^b \int_0^\infty z^d W(z)\,dz}{B} \quad . \tag{34}$$

If the point where the modified fatigue curve intersects the constant-amplitude, sine-wave fatigue curve is assumed to be fixed at σ_1, then the Corten-Dolan theory becomes

$$E(D) = \frac{N_p \sigma_{rms}^d}{A} \int_0^\infty z^d W(z) dz \quad , \tag{35}$$

where

$$A = \sigma_1^{d-b} B \quad .$$

When $E(D) = 1.0$,

$$N_p = \frac{A}{\sigma_{rms}^d \int_0^\infty z^d W(z) dz} \quad . \tag{36}$$

The curve defined by Equation 36 will be parallel to the modified fatigue curve which has a negative slope of 1/d.

At the higher rms stress levels used in this investigation, peak loads occurred which caused the stress to exceed the elastic limit of the material (see Table 3). When a beam is bent into the plastic range, the elastic beam formula no longer applies and the stress distribution across the beam is no longer a straight line. However, the strain distribution across the beam does remain linear and, therefore, the stress distribution takes on the same general shape as the stress versus strain diagram for the material. This is illustrated in Figure 22. For example, with the material used for this

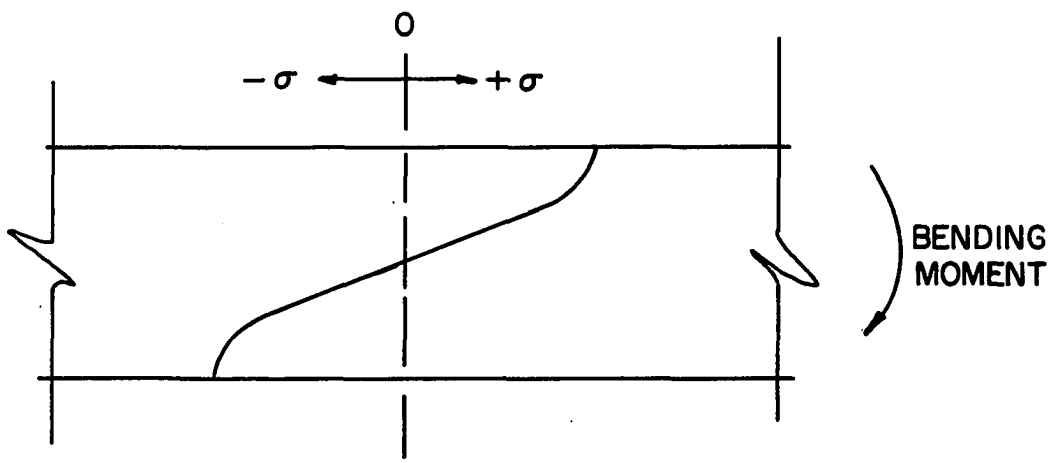

Figure 22. Stress distribution in a plastically deformed beam

investigation, the stress on the surface of the beam will be equal to the yield strength, 51.3 ksi, when a load is applied which would produce an elastic stress of approximately 60 ksi if plastic deformation did not occur. Because of this plastic deformation, the maximum stress on the surface will be approximately equal to the yield strength, $S_{y.s.}$, when overloading occurs. Therefore, the modified fatigue curve was assumed to intersect the regular fatigue curve at the yield strength, i.e., $\sigma_1 = S_{y.s.}$.

Initially it was assumed that stress peaks occurring above σ_1 produced the same fatigue damage as a stress peak equal to σ_1. This gives

$$N_p = \frac{A}{\sigma_1^d \int_{z_1}^{\infty} W(z)dz + \sigma_{rms}^d \int_0^{z_1} z^d W(z)dz} . \qquad (37)$$

This produced a large increase in the predicted fatigue life at the higher stress levels which deviated even further from the experimental results. Therefore, it was assumed that the modified fatigue curve extended above the constant-amplitude, sine-wave fatigue curve, and also, that the damage caused by the stress peaks above σ_1 is the same as if the plastic deformation did not occur. Under these conditions the Corten-Dolan theory is given by Equations 35 and 36.

The expected value of the damage determined from

Equation 35 is given in Table 5 using $\sigma_1 = S_{y.s.}$ and the experimentally determined values of N_p.

Table 5. Expected value of fatigue damage—Corten-Dolan theory

σ_{rms}	Narrow-band E(D)	Broad-band E(D)
26.4	.461	.387
22.7	.397	.391
17.0	.379	.343
13.2	.388	.280
11.3	.374	.391
	Average = .400	Average = .358

The fatigue curves defined by Equation 36 are compared with the experimental results in Figure 23. These curves are very close to being parallel to the experimental fatigue curves, but predict a longer lifetime.

It should be noted that Equation 37 would be applicable when pure clipping of the stress peaks occurs which might result from a limit on the maximum possible deflection of the specimen or of a structure.

Equivalent-Crack-Length Theory

When a metal part or sample is subjected to a repeated or fatigue type of loading, a small crack develops at the surface,

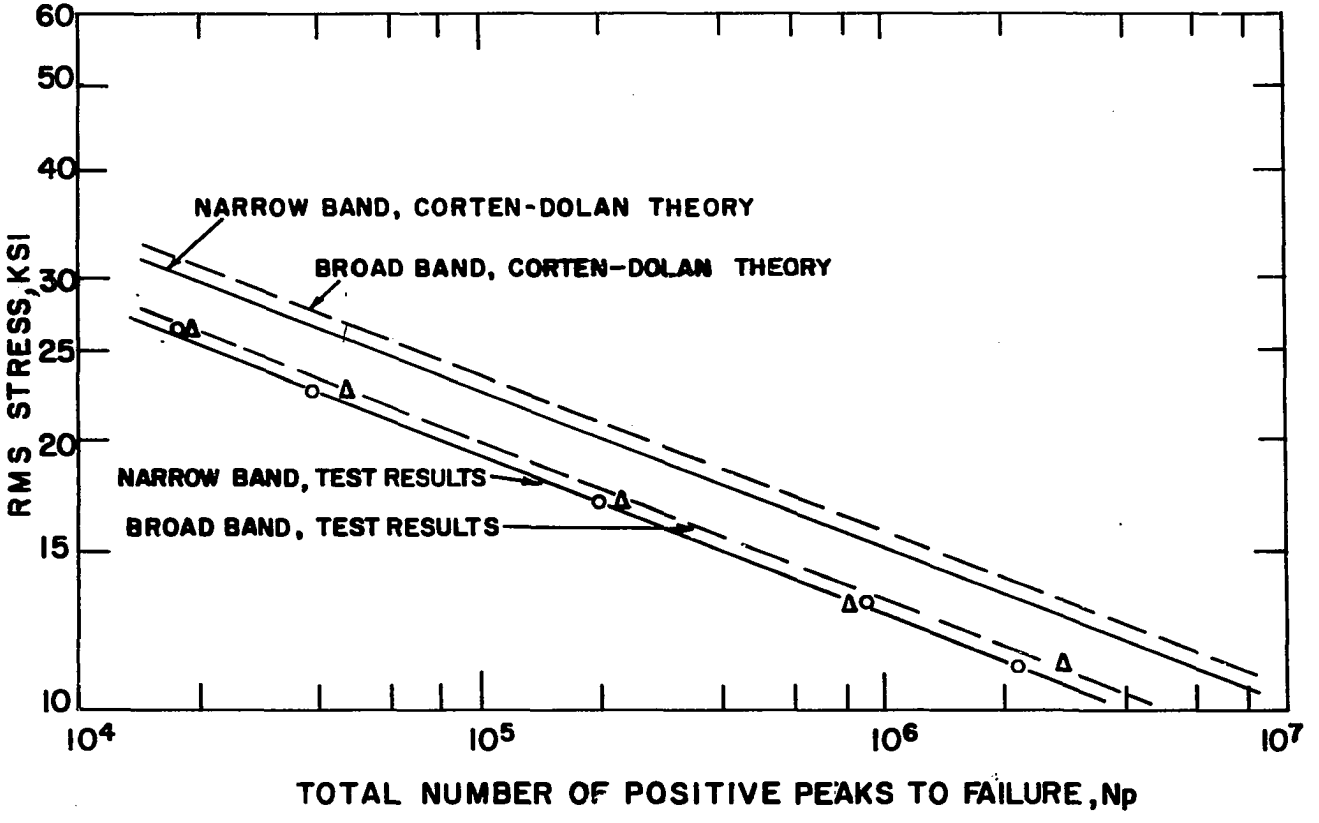

Figure 23. Predicted fatigue life from Corten-Dolan theory

then continues to propagate until the remaining cross sectional area of material is insufficient to withstand the applied stress and fracture results. The generally accepted equation for the rate of fatigue crack propagation under constant-amplitude loading is (38)

$$\frac{d\ell}{dn} = K\sigma^3\ell \quad , \tag{38}$$

where

$\frac{d\ell}{dn}$ = increment of crack growth per cycle,

σ = stress amplitude

ℓ = crack length, and

K = material constant.

Plunkett and Viswanathan (39) found the stress exponent to be 3.08 for 2024-T3 aluminum alloy as compared to 3 used in Equation 38. They also found that under narrow-band random loading the crack growth rate was slower during the earlier stages, nearly equal in the middle range and faster just prior to fracture than that given by Equation 38. However, it is assumed in the following that Equation 38 can be applied over the entire lifetime for the random loading.

In random loading, the fatigue crack grows until a high stress peak occurs that is large enough to fracture the remaining material. It is assumed that the stress peak, σ_1, which causes the failure is the largest peak occurring during

an interval of m cycles. Furthermore, it is assumed that the crack length at failure is the same as the crack length at failure under constant-amplitude loading with stress amplitude, σ_1. The length of this crack is found by integrating Equation 38, which gives,

$$\ell_1 = \ell_0 e^{N_1 K \sigma_1^3} , \tag{39}$$

where N_1 = constant amplitude fatigue life at stress amplitude σ_1. However, since the actual stress amplitude is varying, it is assumed that N_1 is the fatigue life given by the modified fatigue curve,

$$N' \sigma^d = A , \tag{23}$$

which intersects the regular fatigue curve at the yield strength of the material. Therefore,

$$\ell_1 = \ell_0 e^{AK\sigma_1^{3-d}} . \tag{40}$$

Under random loading, the expected value of the crack length after n stress peaks becomes,

$$E(\ell) = \ell_0 e^{nKE(\sigma_p^3)} , \tag{41}$$

where the incremental crack growth is assumed to depend on the magnitude of the stress peak.

Failure will occur when the crack length becomes equal to ℓ_1, therefore, equating $E(\ell)$ to ℓ_1 and solving for n gives,

$$n = \frac{A\sigma_1^{3-d}}{E(\sigma_p)^3} \quad . \tag{42}$$

If only those stress peaks greater than zero contribute to the crack growth, then at failure

$$n = N_{p>0} = N_p \int_0^\infty W(z)dz \quad . \tag{43}$$

where N_p is the total number of positive peaks. Similarily,

$$E(\sigma_p^3) = \frac{\sigma_{rms}^3 \int_0^\infty z^3 W(z)dz}{\int_0^\infty W(z)dz} \quad . \tag{44}$$

Substituting into Equation 42 gives,

$$N_p = \frac{A\sigma_1^{3-d}}{\sigma_{rms}^3 \int_0^\infty z^3 W(z)dz} \quad . \tag{45}$$

With m = 1000, the probability that one peak out of 1000 peaks will be equal to or exceed a stress level, σ_1', is 1/1000. It is assumed that the largest stress peak, σ_1, which occurs

during the 1000 peak interval is equal to the stress level σ_1'. From Equation 30 and the theoretical peak probability density functions shown in Figures 14 and 15, it is found that

$$\sigma_1 = 3.5\sigma_{rms}$$

for both the broad-band and the narrow-band loading. Therefore, Equation 45 becomes

$$N_p = \frac{A}{3.5^{d-3}\sigma_{rms}^{d}\int_0^{\infty} z^3 W(z)dz} , \qquad (46)$$

which defines the fatigue curve for random loading. This curve is compared with the experimental results in Figure 24 for both the narrow-band and broad-band loading.

If σ_1 is assumed to be the largest stress peak which occurs during an interval of 500 peaks instead of 1000 peaks, then a longer lifetime would be predicted. If n_i is the number of peaks to failure predicted by Equation 46 and N_i is the number of peaks predicted by the Corten-Dolan theory, Equation 36, then the expected value of the fatigue damage at failure would be 0.345, which compares with the experimentally-determined average values of 0.400 and 0.358 given in Table 5 for narrow-band and broad-band loading respectively.

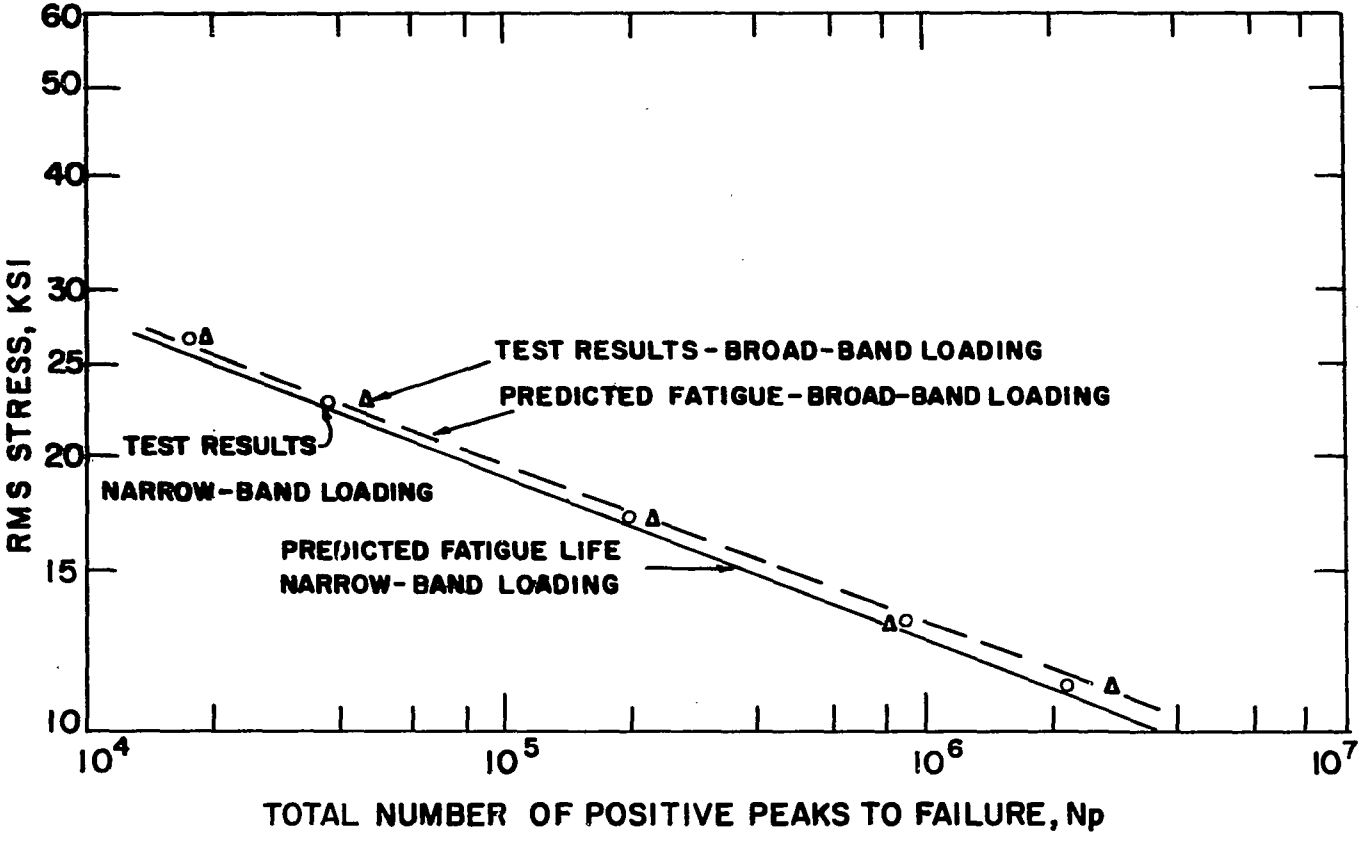

Figure 24. Predicted fatigue life from equivalent crack-length theory

Relation Between Broad-Band and Narrow-Band Loading

It has been shown that both the Palmgren-Miner and the Corten-Dolan theories can be written as

$$\sum_{i=1}^{j} \frac{n_i}{N_i} = 1 \quad . \tag{47}$$

The difference between the two depends on whether the regular fatigue curve or the modified fatigue curve is used to determine N_i. Let the fatigue curve be represented by the equation

$$N\sigma^{\theta} = F \quad , \tag{48}$$

where $\theta = b$ for the Palmgren-Miner theory and $\theta = d$ for the Corten-Dolan theory. Substituting N from Equation 48 into Equation 47 gives,

$$\sum_{i=1}^{j} \frac{n_i \sigma_i^{\theta}}{F} = 1 \quad . \tag{49}$$

The incremental damage, D_i, caused by stress σ_i is then

$$D_i = \frac{n_i \sigma_i^{\theta}}{F} \quad . \tag{50}$$

From this, it is seen that the damage is weighted according to the stress raised to the θ power. The consistent results of Corten and Dolan which showed the slope of the modified fatigue curve to be the same for different levels of stress, suggests that d would be the better choice for the value of θ.

With $\theta = d$, Equation 50 indicates that a comparison between different types of random loading (different power spectral densities) should be based on the peak stress raised to the d power. This can be done by plotting $[E(\sigma^d_{p>0})]^{1/d}$ versus log $N_{p>0}$, where again only the peaks greater than zero are assumed to contribute to the fatigue damage. The 1/d root of the expected value is used only to provide a convenient scale. The expected value of $\sigma^d_{p>0}$ is

$$E(\sigma^d_{p>0}) = \frac{\sigma^d_{rms}\int_0^\infty z^d W(z)\,dz}{\int_0^\infty W(z)\,dz} , \qquad (51)$$

and $N_{p>0}$ is

$$N_{p>0} = N_p\int_0^\infty W(z)\,dz . \qquad (52)$$

Therefore, the data for different types of random loading should fall on a single line by plotting $[E(\sigma^d_{p>0})]^{1/d}$ versus log $N_{p>0}$. This is illustrated in Figure 25 for the test results of this investigation.

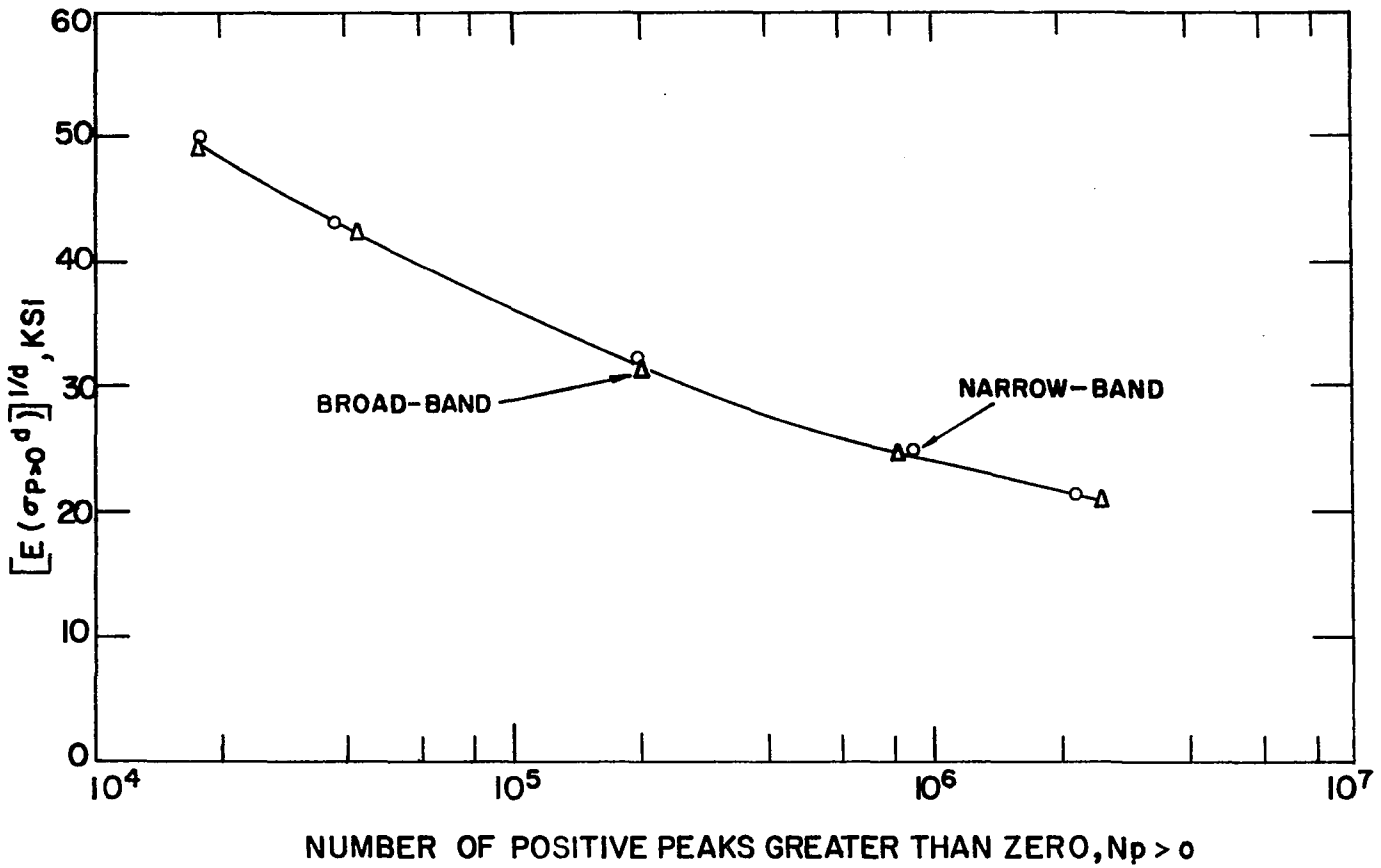

Figure 25. $\left[E(\sigma_{p>0})^d\right]^{1/d}$ versus $N_{p>0}$

Comparison with Fuller's test results

Fuller (21) conducted random fatigue tests on 2024-T3 aluminum alloy using the three different power spectrums shown in Figure 26.

The $[E(\sigma^d_{p>0})]^{1/d}$ is plotted against log $N_{p>0}$ in Figure 27, where d was assumed to 0.85 times the value of b determined from the log σ versus log N curve for the constant-amplitude, sine-wave tests conducted by Fuller.

The results shown in Figure 25 for the tests of this investigation and Fuller's results shown in Figure 27 show that this is a satisfactory means of comparing fatigue life under different types of random loading.

If the fatigue curve for one type of random loading is known, then the fatigue life for a different type of loading can be found by knowing the Corten-Dolan constant, d, and the peak probability density function. It is considerably easier to build fatigue testing equipment for random fatigue testing under resonance conditions which gives a narrow-band type of loading. Therefore, test results from such equipment could be used for predicting the fatigue life under other types of random loading.

This approach should be investigated for other types of random loading with smaller ratios of N_0/M.

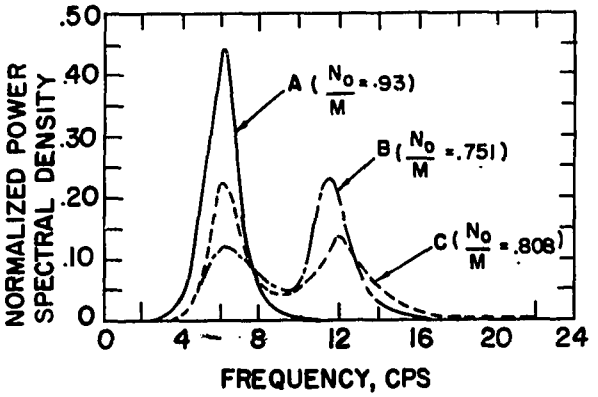

Figure 26. Power spectrums used by Fuller (21)

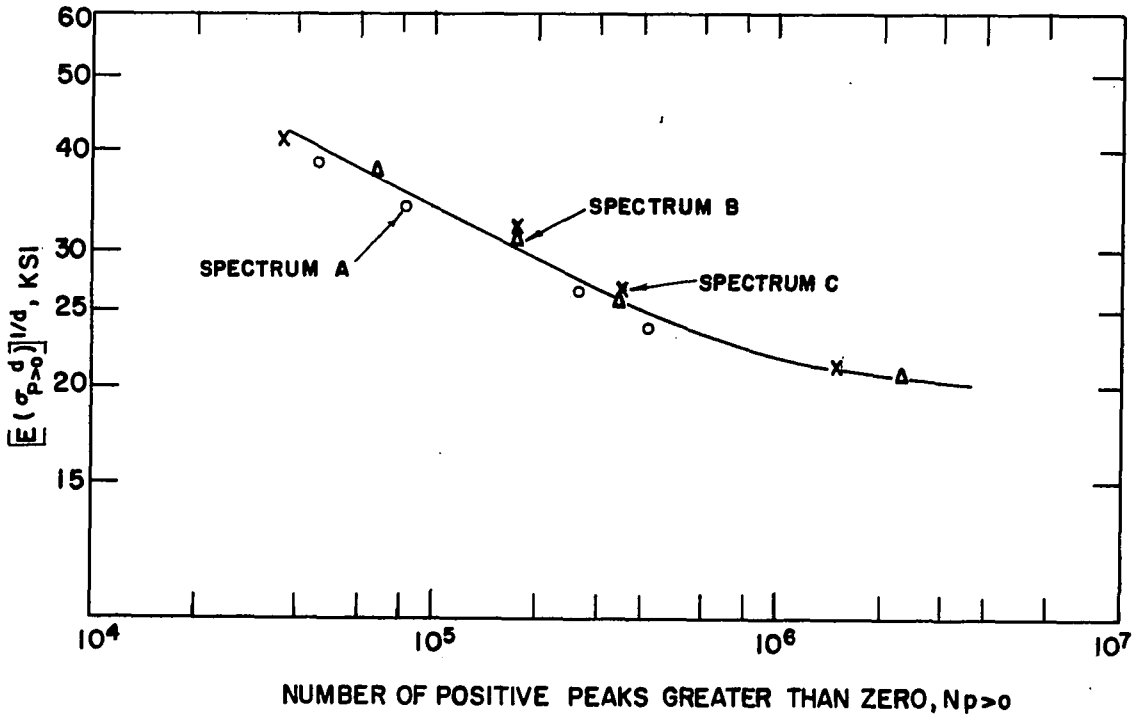

Figure 27. $\left[E(\sigma^d_{p>0})\right]^{1/d}$ versus $N_{p>0}$ for Fuller's test results

CONCLUSIONS

The test results show that the random fatigue curves for the two types of loading are nearly parallel. The broad-band loading gives a slightly greater number of peaks to failure. It appears that as the ratio N_0/M decreases, the fatigue curve is displaced to the right indicating a longer lifetime. This is in general agreement with Fuller's results. Also, the random fatigue curves are very nearly parallel to the modified fatigue curve defined for the Corten-Dolan theory.

The random fatigue curve predicted by the Palmgren-Miner theory is parallel to the constant-amplitude, sine-wave curve and predicts lifetimes of 1.5 to 5 times those observed. This is in agreement with results of other investigations and shows that the Palmgren-Miner theory overestimates the fatigue life and should not be used for random loading.

The Corten-Dolan theory gives a fatigue curve parallel to the constant-amplitude, sine-wave fatigue curve and parallel to the Palmgren-Miner curve if the maximum possible stress peak is not limited during the stress history. If the maximum stress peak is assumed to be fixed for different rms stress levels, then the predicted curve is parallel to the modified fatigue curve. With this assumption, the Corten-Dolan theory overestimates the lifetime by about 2.5.

For the equivalent-crack-length theory, it is assumed that failure is caused by the largest stress peak which occurs

in an interval of 1000 stress peaks and that the crack length at failure will be the same as that at failure given by the modified fatigue curve. This theory gives excellent agreement with the test results for both the broad- and narrow-band random loading.

The concept that early fracture is caused by a high stress peak accounts for the shorter lifetime than that predicted by the Palmgren-Miner and Corten-Dolan theories. This concept of early failure is in agreement with the results of most of the other investigations that have been made. This is further substantiated by the test results of Girks (22) who defined fatigue failure to be when the fatigue crack had grown to a certain length. He found the Palmgren-Miner theory to give a good prediction of the fatigue life. Thus it appears that the fatigue damage due to random loading accumulates according to the Palmgren-Miner theory, but a large stress peak occurs which causes fracture earlier than expected.

Good correlation for the two different types of random loading was found by plotting $[E(\sigma_{p>0}^{d})]^{1/d}$ versus $N_{p>0}$. This not only gives a convenient means of comparing different types of random loading, but also shows that fatigue damage accumulates according to the stress peaks raised to the d power and only those peaks above zero contribute to this damage. Therefore, these appear to be the most significant factors influencing the fatigue behavior under random loading.

RECOMMENDATIONS FOR FURTHER STUDY

The proposed equivalent-crack-length theory and the method of comparing the fatigue life under different types of random loading should be compared with test results using random loading with a smaller ratio for $N_0/_M$. This type of random loading could be obtained by filtering the noise input with two narrow-pass filters where the higher frequency filter has a lower gain.

The use of the magnitude and the number of the positive peaks greater than zero as the statistical quantities for comparing different types of random loading could be investigated further by conducting tests with different power spectral densities, but with the same ratio of $N_0/_M$. Since the peak probability density curves would be the same, the fatigue life should be the same for the different power spectrums. An immediate investigation would be to use a filter as described above, which gives the same ratio of $N_0/_M$ as for the broad-band loading used in this investigation.

The effect of stressing below the endurance limit for a portion of the lifetime has been a topic of considerable interest for some time, particularly for steel which has a definite infinite-life region. The ability to determine the number of peak stresses occurring below a certain level from the peak probability density function suggests that this could be determined using random loading.

The test equipment used in this investigation could be used for testing under a multitude of different types of stress-time histories. It could readily be used for testing with recordings of actual service loadings.

It is recommended that improvements be made in the pinned connection before additional tests are conducted with this equipment, since after several tests the pin becomes loose and causes high frequency vibrations. This was overcome by periodically replacing a small shim inserted in the connection.

Extreme care should be taken in machining the specimens because of their small size.

LITERATURE CITED

1. Moore, H. F. and Kommers, J. B. The fatigue of metals. McGraw-Hill Book Company, Inc., New York, N.Y. 1927.

2. Palmgren, A. Die Lebensdauer von Kugellagern. Vereines Deutscher Ingenieure Zeitschrift 68, No. 14: 339-341. 1924.

3. Miner, M. A. Cumulative damage in fatigue. Jour. Appl. Mech. 12: A159-A164. 1945.

4. Dolan, T. J., Richart, F. E. and Work, C. E. Influence of fluctuations in stress amplitude on the fatigue of metals. Am. Soc. Test. Mat. Proc. 49: 646-682. 1949.

5. Naumann, E. C., Hardrath, H. F. and Guthrie, D. E. Axial-load fatigue tests of 2024-T3 and 7075-T6 aluminum-alloy sheet specimens under constant- and variable-amplitude loads. U.S. Nat. Aero. and Space Admin. Tech. Note D-212. 1959.

6. Naumann, E. C. and Schott, R. L. Axial-load fatigue tests using loading schedules based on maneuver-load statistics. U.S. Nat. Aero. and Space Admin. Tech. Note D-1253. 1952.

7. Freudenthal, A. M. and Heller, R. A. On stress interaction in fatigue and a cumulative damage rule. Jour. Aero-Space Sci. 26: 431-442. 1959.

8. Corten, H. T. and Dolan, T. J. Cumulative fatigue damage. In Int. Conf. on Fatigue of Metals Proc. pp. 235-246. Institute of Mechanical Engineers, London, England. 1956.

9. Valluri, S. R. A unified engineering theory of high stress level fatigue. Aerospace Eng. 20, No. 10: 18-19, 68-89. 1961.

10. Freudenthal, A. M. Random fatigue testing procedure and machine. Am. Soc. Test. Mat. Proc. 53: 896-910. 1953.

11. Miner, M. A. Estimation of fatigue life with particular emphasis on cumulative damage. In Sines, G. and Waisman, J. L., eds. Metal fatigue. pp. 278-289. McGraw-Hill Book Company, Inc., New York, N.Y. 1959.

12. Head, A. K. and Hooke, F. H. Random noise fatigue testing. In Int. Conf. on Fatigue of Metals Proc. pp. 301-303. Institute of Mechanical Engineers, London, England. 1956.

13. McIntosh, V. C. and Granick, N. Experiments in random vibrations. Wright Air Development Center Tech. Note 56-228. 1956. Original not available; cited in Swanson, S. R. An investigation of the fatigue of aluminum alloy due to random loading. Univ. Toronto Inst. Aerophysics UTIA Report No. 84: 60. 1963.

14. Smith, P. W. and Malme, C. I. Fatigue tests of a resonant structures with random excitation. Acoustical Soc. Am. Jour. 35: 43-46. 1963.

15. Trotter, W. D. Fatigue of 2024-T3 aluminum sheet under random loading. Boeing Airplane Co. Test Rep. No. T2-1601. 1958.

16. Fralich, R. W. Experimental investigation of effects of random loading on the fatigue life of notched cantilever-beam specimens of 7075-T6 aluminum alloy. U.S. Nat. Aero. and Space Admin. Memo. 4-12-59L. 1959.

17. Fralich, R. W. Experimental investigation of effects of random loading on the fatigue life of notched cantilever-beam specimens of SAE 4130 normalized steel. U.S. Nat. Aero. and Space Admin. Tech. Note D-663. 1961.

18. Kowalewski, J. On the relation between fatigue lives under random loading and corresponding program loading. In Plantema, F. J. and Schijve, J., eds. Full-scale fatigue testing of aircraft structures. pp. 60-75. Pergamon Press, Ltd., New York, N.Y. 1961.

19. Crichlow, W. J. et al. An engineering evaluation of methods for the prediction of fatigue life in airframe structures. Aero. Systems Div. Tech. Rep. 61-434. March, 1952. Original not available; cited in Swanson, S. R. An investigation of the fatigue of aluminum alloy due to random loading. Univ. Toronto Inst. Aerophysics UTIA Rep. No. 84: 61. 1963.

20. Swanson, S. R. An investigation of the fatigue of aluminum alloy due to random loading. Univ. Toronto Inst. Aerophysics UTIA Rep. No. 84. 1963.

21. Fuller, J. R. Research on techniques of establishing random type fatigue curves for broad band sonic loading. Soc. Auto. Engr. and Am. Soc. Naval Engr. [Joint Publishers] Paper 671C. 1963.

22. Girks, I. F. Optimization of testing time. U.S. Nat. Aero. Space Admin. Contract Report 77338. 1966.

23. Hillberry, B. M. Broad-band, random-load fatigue testing system. Unpublished M.S. thesis. Library, Iowa State University of Science and Technology, Ames, Iowa. 1964.

24. Taylor, J. Fatigue loading actions on transport aircraft. In Int. Conf. on Fatigue of Metals Proc. pp. 650-657. Institute of Mechanical Engineers, London, England. 1956.

25. Vigness, I. Field measurements, specifications, and testing. In Crandall, S. H., ed. Random vibration. Vol. 2. pp. 195-242. Massachusetts Institute of Technology Press, Cambridge, Mass. 1963.

26. Scouten, D. C. Use of composite complementary-symmetry transistors in precise linear power amplification. Unpublished Ph.D. thesis. Library, Iowa State University of Science and Technology, Ames, Iowa. 1963.

27. American Society for Testing Materials. Committee E-9 on Fatigue. Manual on fatigue testing. Am. Soc. Test. Mat. Spec. Tech. Publ. No. 91. 1948.

28. Brown, R. G. and Nilsson, J. W. Introduction to linear systems analysis. John Wiley and Sons, Inc., New York, N.Y. 1962.

29. General Radio Company. Operating instructions manual: type 1390-B random noise generator. Author, West Concord, Mass. 1964.

30. Hansen, P. D. New approaches to the design of active low pass filters. Lightening Empiricist 13, No. 3: 2-12. 1965.

31. Rice, S. O. Mathematical analysis of random noise. Part 2. Bell system Tech. Jour. 24, No. 1: 46-150. 1945.

32. Bendat, J. S. Probability functions for random responses: prediction of peaks, fatigue damage, and catastrophic failures. U.S. Nat. Aero. Space Admin. Contract Report 33. 1964.

33. Counter, L. F. Investigation of dynamic characteristics and capabilities of a broad-band, random-load fatigue testing facility. Unpublished M.S. thesis. Library, Iowa State University of Science and Technology, Ames, Iowa. 1966.

34. Forrest, P. G. Fatigue of metals. Addison-Wesley Publishing Co., Inc., Reading, Mass. 1962.

35. Christensen, R. H. Fatigue cracking, fatigue damage and their detection. In Sines, G. and Waisman, J. L., eds. Metal fatigue. pp. 376-412. McGraw-Hill Book Company, Inc., New York, N.Y. 1959.

36. Crandall, S. H. and Mark, W. D. Random vibration in mechanical systems. Academic Press., New York, N.Y. 1963.

37. Root, L. W. Selection of vibration test levels using fatigue criteria. Unpublished paper presented at Thirty-fourth Symposium on Shock, Vibration and Associated Environments, Fort Ord, Calif., 1964. Collins Radio Company, Cedar Rapids, Iowa. 1964.

38. Hardrath, H. F. Fatigue of metals: part 2, crack propagation and final failure. Mat. Res. Std. 3: 116-121. 1963.

39. Plunkett, R. and Viswanathan, N. Fatigue-crack-propagation rates under random excitation. Unpublished paper No. 66-WA/MET-3 presented at Am. Soc. Mech. Engr. Winter Annual Meeting, New York, N.Y., Nov., 1966. Am. Soc. Mech. Engr., New York, N.Y. 1966.

40. Jahnke, E. and Emde, F. Tables of functions with formulae and curves. 4th ed. Dover Publications, Inc., New York, N.Y. 1945.

ACKNOWLEDGMENTS

The author wishes to express his appreciation to Professor H. M. Black, who served as chairman of the author's graduate study committee, and to Dr. R. G. Brown, who served as co-chairman, for their assistance throughout this program.

The cooperation of Mr. I. F. Girks, Collins Radio Company, who assisted with measuring the power spectrums and probability densities, is gratefully acknowledged.

The financial support provided by the E. I. du Pont de Nemours & Company is acknowledged.

A special note of appreciation is extended to the author's wife and family for their patience and understanding throughout the years of graduate study.

APPENDIX

Evaluation of $\int_0^\infty z^b W(z)\,dz$

Narrow-band loading

For narrow-band random loading, $N_0/M = 1.0$, and therefore,

$$W(z) = ze^{-\frac{z^2}{2}} \tag{A.1}$$

This gives

$$\int_0^\infty z^b W(z)\,dz = \int_0^\infty z^{b+1}\, e^{-\frac{z^2}{2}}\, dz \quad , \tag{A.2}$$

which reduces to the gamma function,

$$\int_0^\infty z^{b+1}\, e^{-\frac{z^2}{2}}\, dz = z^{\frac{b}{2}}\, \Gamma\left(\frac{b}{2}+1\right) \quad . \tag{A.3}$$

Broad-band random loading

For broad-band loading the peak probability density function is given by Equation 6. Substituting into the integral gives

$$\int_0^\infty z^b W(z)\,dz = \int_0^\infty \left\{ \frac{K_1}{\sqrt{2\pi}} z^b e^{-\frac{z^2}{2K_1^2}} + \frac{N_0}{M} z^{b+1}\, e^{-\frac{z^2}{2}} \left[1-P\left(\frac{z}{K_2}\right) \right] \right\} dz \quad , \tag{A.4}$$

where

$$P\left(\frac{z}{K_2}\right) = \frac{1}{\sqrt{2\pi}} \int_{\frac{z}{K_2}}^{\infty} e^{-\frac{y^2}{2}}\, dy \quad .$$

Substituting in for $P\left(\frac{z}{K_2}\right)$ gives

$$\int_0^{\infty} z^b W(z)\, dz = \frac{K_1}{\sqrt{2\pi}} \int_0^{\infty} z^b\, e^{-\frac{z^2}{2K_1^2}}\, dz + \frac{N_0}{M} \int_0^{\infty} z^{b+1}\, e^{-\frac{z^2}{2}}\, dz$$

$$- \frac{N_0}{M\sqrt{2\pi}} \int_0^{\infty} z^{b+1}\, e^{-\frac{z^2}{2}} \int_{\frac{z}{K_2}}^{\infty} e^{-\frac{y^2}{2}}\, dy dz \quad . \qquad \text{(A.5)}$$

Let the first, second and third integrals of Equation A.5 equal I_1, I_2 and I_3, respectively. Changing variables of integration in I_1 gives the gamma function,

$$I_1 = 2^{\frac{b-1}{2}} K_1^{b+1}\, \Gamma\left(\frac{b+1}{2}\right) \quad . \qquad \text{(A.6)}$$

Similarily for I_2,

$$I_2 = 2^{\frac{b}{2}}\, \Gamma\left(\frac{b}{2}+1\right) \quad . \qquad \text{(A.7)}$$

Changing the order of integration of the double integral, I_3, yields

$$I_3 = \int_0^{\infty} e^{-\frac{y^2}{2}} \int_0^{yK_2} z^{b+1} e^{-\frac{z^2}{2}} dzdy \quad . \qquad (A.8)$$

If b+1 is an odd integer, successively integrating by parts will reduce the integral of Equation A.8 to the gamma function. If b+1 is an even integer, then successively integrating by parts reduces I_3 to,

$$I_3 = \int_0^{\infty} e^{-\frac{y^2}{2}} \int_0^{yK_2} e^{-\frac{z^2}{2}} dzdy + C \quad , \qquad (A.9)$$

which can be integrated by changing to polar coordinates.

When b+1 is not an integer, the integral on z in Equation A.8 can be written as,

$$\int_0^{yK_2} z^{b+1} e^{-\frac{z^2}{2}} = 2^{\frac{b}{2}} \int_0^{\frac{y^2K_2^2}{2}} t^{\frac{b}{2}} e^{-t} dt \quad , \qquad (A.10)$$

by changing variables of integration. This is the incomplete gamma function which can be expanded into a power series (40),

$$\int_0^{yK_2} z^{b+1} e^{-\frac{z^2}{2}} dz = \sum_{n=0}^{\infty} \frac{(-1)^n (K_2y)^{b+2+2n}}{2^{n+1} n! \left(\frac{b}{2}+n+1\right)} \quad . \qquad (A.11)$$

Substituting this into Equation A.8 and moving the integral on y inside the summation results in the gamma function and I_3 becomes,

$$I_3 = 2^{\frac{b-1}{2}} \sum_{n=0}^{\infty} \frac{(-1)^n K_2^{b+2+2n} \Gamma\left(\frac{b}{2}+n+\frac{3}{2}\right)}{2^{n+1} n! \left(\frac{b}{2}+n+1\right)} \quad . \qquad \text{(A.12)}$$

Therefore,

$$\int_0^{\infty} z^b W(z)\,dz = \frac{K_1}{\sqrt{2\pi}} I_1 + \frac{N_0}{M} I_2 - \frac{N_0}{M\sqrt{2\pi}} I_3 \quad , \qquad \text{(A.13)}$$

where I_1, I_2 and I_3 are given by Equations A.6, A.7 and A.12, respectively.

A computer program was written to evaluate this equation. Forty terms were sufficient for the convergence of the series.